



**UNIVERSIDAD DE INVESTIGACIÓN DE TECNOLOGÍA  
EXPERIMENTAL YACHAY**

**Escuela de Ciencias Químicas e Ingeniería**

**TÍTULO: REMOVAL OF POTENTIALLY TOXIC METALS BY  
USING LOW COST BIO-ADSORBENTS PREPARED FROM  
AGRICULTURAL WASTE**

Trabajo de integración curricular presentado como requisito para la  
obtención del título de QUÍMICO/A

**Autor:**

Parra Quisahuano Dolores Lastenia

**Tutor:**

Ph.D. López González Floralba Aggeny

Urququí, Septiembre 2019

**SECRETARÍA GENERAL**  
**(Vicerrectorado Académico/Cancillería)**  
**ESCUELA DE CIENCIAS QUÍMICAS E INGENIERÍA**  
**CARRERA DE QUÍMICA**  
**ACTA DE DEFENSA No. UITEY-CHE-2019-00005-AD**

En la ciudad de San Miguel de Urcuquí, Provincia de Imbabura, a los 23 días del mes de agosto de 2019, a las 10:00 horas, en el Aula AI-101 de la Universidad de Investigación de Tecnología Experimental Yachay y ante el Tribunal Calificador, integrado por los docentes:

<b>Presidente Tribunal de Defensa</b>	Dr. SAUCEDO VAZQUEZ, JUAN PABLO, Ph.D.
<b>Miembro No Tutor</b>	Dr. THIBAUT TERENCIO, Ph.D.
<b>Tutor</b>	Dra. LOPEZ GONZALEZ, FLORALBA AGGENY, Ph.D.

Se presenta el(la) señor(ita) estudiante PARRA QUISAHUANO, DOLORES LASTENIA, con cédula de identidad No. 1724149370, de la ESCUELA DE CIENCIAS QUÍMICAS E INGENIERÍA, de la Carrera de QUÍMICA, aprobada por el Consejo de Educación Superior (CES), mediante Resolución RPC-SO-39-No.456-2014, con el objeto de rendir la sustentación de su trabajo de titulación denominado: **Removal of potentially toxic metals by using low cost bio-adsorbents prepared from agricultural waste**, previa a la obtención del título de QUÍMICO/A.

El citado trabajo de titulación, fue debidamente aprobado por el(los) docente(s):

<b>Tutor</b>	Dra. LOPEZ GONZALEZ, FLORALBA AGGENY, Ph.D.
--------------	---

Y recibió las observaciones de los otros miembros del Tribunal Calificador, las mismas que han sido incorporadas por el(la) estudiante.

Previamente cumplidos los requisitos legales y reglamentarios, el trabajo de titulación fue sustentado por el(la) estudiante y examinado por los miembros del Tribunal Calificador. Escuchada la sustentación del trabajo de titulación, que integró la exposición de el(la) estudiante sobre el contenido de la misma y las preguntas formuladas por los miembros del Tribunal, se califica la sustentación del trabajo de titulación con las siguientes calificaciones:

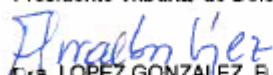
Tipo	Docente	Calificación
Presidente Tribunal De Defensa	Dr. SAUCEDO VAZQUEZ, JUAN PABLO, Ph.D.	9,8
Tutor	Dra. LOPEZ GONZALEZ, FLORALBA AGGENY, Ph.D.	9,8
Miembro Tribunal De Defensa	Dr. THIBAUT TERENCIO, Ph.D.	9,6

Lo que da un promedio de: **9.7 (Nueve punto Siete)**, sobre 10 (diez), equivalente a: **APROBADO**

Para constancia de lo actuado, firman los miembros del Tribunal Calificador, el(la) estudiante y el(la) secretario ad-hoc.

  
**PARRA QUISAHUANO, DOLORES LASTENIA**  
 Estudiante

  
 Dr. SAUCEDO VAZQUEZ, JUAN PABLO, Ph.D.  
 Presidente Tribunal de Defensa

  
 Dra. LOPEZ GONZALEZ, FLORALBA AGGENY, Ph.D.  
 Tutor





**Dr. THIBAULT TERCENIO, Ph.D.**  
**Miembro No Tutor**

**ESCOBAR LANDAZURI, ANA MARIA**  
**Secretario Ad-hoc**

## AUTORÍA

Yo, **DOLORES LASTENIA PARRA QUISAHUANO**, con cédula de identidad 1724149370, declaro que las ideas, juicios, valoraciones, interpretaciones, consultas bibliográficas, definiciones y conceptualizaciones expuestas en el presente trabajo; así cómo, los procedimientos y herramientas utilizadas en la investigación, son de absoluta responsabilidad de el/la autora (a) del trabajo de integración curricular. Así mismo, me acojo a los reglamentos internos de la Universidad de Investigación de Tecnología Experimental Yachay.

Urququí, Septiembre 2019.



Dolores Lastenia Parra Quisahuano

CI: 1724149370

## AUTORIZACIÓN DE PUBLICACIÓN

Yo, **DOLORES LASTENIA PARRA QUISAHUANO**, con cédula de identidad 1724149370, cedo a la Universidad de Tecnología Experimental Yachay, los derechos de publicación de la presente obra, sin que deba haber un reconocimiento económico por este concepto. Declaro además que el texto del presente trabajo de titulación no podrá ser cedido a ninguna empresa editorial para su publicación u otros fines, sin contar previamente con la autorización escrita de la Universidad.

Asimismo, autorizo a la Universidad que realice la digitalización y publicación de este trabajo de integración curricular en el repositorio virtual, de conformidad a lo dispuesto en el Art. 144 de la Ley Orgánica de Educación Superior

Urcuquí, Septiembre 2019.



Dolores Lastenia Parra Quisahuano

CI: 1724149370

## **Dedicatoria**

A la memoria de mi padre Juan y mis abuelos María y Leonardo.

Este trabajo está dedicado a mi madre Aída y mis hermanos Ale y Danny quienes siempre me han apoyado incondicionalmente durante este proceso.

A mis amigos que me apoyaron hasta que este sueño se hizo realidad.

Dolores Lastenia Parra Quisahuano

## **Agradecimientos**

A mis tutores Ph.D. Floralba López y Ph.D. Gottfried Suppan por sus enseñanzas y orientación durante el desarrollo de este proyecto de investigación.

Al Ph.D. Juan Carlos Moreno y el Laboratorio de Materiales de la Universidad de Austria por los análisis de XPS.

A la Ph.D. Paulina Romero y al Laboratorio de Nuevos Materiales de la Escuela Politécnica Nacional por su colaboración con los análisis de los espectros Raman.

Al Ph.D. Terencio Thibault por brindarme su ayuda durante la medición de los espectros de UV-VIS.

Al Ph.D. Juan Pablo Saucedo por sus consejos durante el desarrollo de la investigación.

A todos los profesores de la Universidad Yachay Tech que me han brindado sus conocimientos para mi desarrollo intelectual.

Dolores Lastenia Parra Quisahuano

## ABSTRACT

This research work proposes the harnessing of agricultural wastes from the Province of Imbabura-Ecuador for the preparation of adsorbents for potentially toxic metal removal from aqueous solutions. This study has the purpose of generating adsorbent filters for the bio-remediation of natural water bodies where the effluents, originated from textile, leather tanning and mining industry, are discharged. Specifically, it is used corn stalk as raw material, for which it is considered the optimization of performance, savings in the material used, as well as involving the use and re-valuation of waste resources, fostering interest in the development of adsorbents from Biomass. Due to its chemical structure, the lignin, one of the principal biomass constituents present in the raw materials, is a key component in the activity proposed. To quantify the adsorptive capability of adsorbent rich in lignin, the decreasing concentration of evaluated metal solutions after being in contact with the adsorbent was measured using different analytical methods with sufficiently low detection limits, such as UV-VIS Spectroscopy and Anodic Stripping Voltammetry (ASV). From the analysis of the Isotherms of adsorption, it was possible to infer about the nature of adsorption (chemical or physical) involved, in understanding the mechanism/interaction between solid and metal species, responsible for the removal of the metal ions. The results showed that environmental toxic metal contaminants, such as  $\text{Ni}^{2+}$  and  $\text{Co}^{2+}$ , can be successfully removed. Finally, the characterization of the resultant lignin-metal compound was performed using spectroscopic techniques such as Raman and X-ray photoelectron spectroscopy (XPS). The processes of solid characterization show the presence of lignin, the reduction of nickel ion and a possible formation of nickel carbide.

**Keywords:** Toxic metals, biomass, bio-adsorbents, wastewater, industrial process, adsorption process.

## RESUMEN

Este trabajo de investigación propone el aprovechamiento de los desechos agrícolas de la provincia de Imbabura-Ecuador para la preparación de adsorbentes para la eliminación de metales potencialmente tóxicos de las soluciones acuosas. Este estudio tiene el propósito de generar filtros adsorbentes para la biorremediación de cuerpos de agua naturales donde se descargan los efluentes originarios de la industria textil, curtidora de cuero y minería. Específicamente, se utiliza el tallo del maíz como materia prima, por lo que se considera la optimización del rendimiento, el ahorro en el material utilizado, así como el uso y la revaluación de los recursos de residuos, lo que fomenta el interés en el desarrollo de adsorbentes a partir de biomasa. Debido a su estructura química, la lignina, uno de los principales componentes de la biomasa presente en las materias primas, es un componente clave en la actividad propuesta. Para cuantificar la capacidad de adsorción del adsorbente rico en lignina, la concentración decreciente de las soluciones metálicas evaluadas después de estar en contacto con el adsorbente se midió utilizando diferentes métodos analíticos con límites de detección suficientemente bajos, como la espectroscopia UV-VIS y la voltametría de separación anódica (ASV). A partir del análisis de las isotermas de adsorción, fue posible inferir sobre la naturaleza de la adsorción (química o física) involucrada, en la comprensión del mecanismo/interacción entre especies sólidas y metálicas, responsables de la eliminación de los iones metálicos. Los resultados mostraron que los contaminantes metálicos tóxicos ambientales, como  $\text{Ni}^{2+}$  y  $\text{Co}^{2+}$ , pueden eliminarse con éxito. Finalmente, la caracterización del compuesto resultante de lignina-metal se realizó utilizando técnicas espectroscópicas tales como Raman y espectroscopia de fotoelectrones de rayos X (XPS). Los procesos de caracterización sólida muestran la presencia de lignina, la reducción del ion níquel y una posible formación de carburo de níquel.

**Palabras clave:** metales tóxicos, biomasa, bio-adsorbentes, aguas residuales, procesos industriales, procesos de adsorción.

## TABLE OF CONTENTS

TABLE OF CONTENTS.....	1
LIST OF ABBREVIATION.....	2
1. INTRODUCTION – JUSTIFICATION:.....	3
2. PROBLEM STATEMENT:.....	5
3. GENERAL AND SPECIFIC OBJECTIVES:.....	5
3.1 General Objective.....	5
3.2 Specific Objectives.....	5
4. METHODOLOGY.....	6
4.1 Reagents, Materials and Equipment.....	6
4.2 Theoretical Background.....	6
4.3 Experimental Procedure A - Adsorption Process Stage.....	10
4.3.1 Adsorbent preparation.....	10
4.3.2 Solution preparation.....	10
4.3.3 Adsorption process.....	10
4.4 Experimental Procedure B - Solution Characterization Stage.....	11
4.4.1. UV-Visible Spectroscopy.....	12
4.4.2. Voltammetry.....	12
4.2.2.1 Cyclic voltammetry.....	13
4.2.2.2 Linear sweep voltammetry.....	13
4.5 Experimental Procedure C - Solid Characterization Stage.....	14
4.5.1 X-ray Photoelectron Spectroscopy (XPS).....	14
4.5.2 Raman spectroscopy (RaS).....	15
5. RESULTS, INTERPRETATION AND DISCUSSION.....	16
5.1 Preparation of calibration curves.....	16
5.2 Measurements of [Ni <sup>2+</sup> ] by UV-Spectroscopy and Voltammetry after of the Adsorption Process.....	23
5.2.1 Isotherms.....	25
5.3 Measurements of [Co <sup>2+</sup> ] by UV-Spectroscopy and Voltammetry after adsorption process ..	28
5.3.1 Isotherms.....	29
5.3.2 Other Isotherms - Cobalt Solutions.....	30
5.4 Solid Characterization.....	32
6. CONCLUSIONS AND RECOMMENDATIONS.....	41
7. BIBLIOGRAPHY.....	42
8. ANNEX.....	46

## **LIST OF ABBREVIATION**

UV-Vis	UV-Visible spectroscopy
XPS	X-ray photoelectron spectroscopy
AP	Adsorption process
CC	Calibration curve
AW	Agricultural waste

## 1. INTRODUCTION – JUSTIFICATION:

Water is a primordial component for nature. It is of essential importance for sustaining and reproducing life on the planet. Water pollution destroys the equilibrium of living organisms and the environment. Therefore, finding a solution to this problem is a vitally important need.

One of the source of pollution of water is the accumulation of several harmful substances of industrial activities, which are discharge to the body of waters in different ways: continuously, intermittently or randomly. Industrial wastes include the presence of chemical compounds related to contamination and potential toxicity, sometimes called heavy metals. Although some of these elements may be present in trace concentrations, their presence has a strong negative impact on the environment, even generating a public health problem. In other cases, some of these could be part of the natural ecosystem, but high concentrations can cause several damages to the environment.

According to Equatorian Legislations, such as the *Norma de Calidad Ambiental y de Descarga de Efluentes: Recurso Agua* established in 2010<sup>1</sup>, as well as the *Texto Unificado de Legislación Secundaria del Medio Ambiente* (TULSMA)<sup>2</sup>, the quality criteria for the preservation of flora and fauna in cool or warm freshwater establish the maximum permissible limits of some chemical compounds, whose specific values for some metals are shown in the Table 1. However, it has been found in several sampling stations that the content of the metals exceeds the maximum permissible limits, for example in the Santiago river of the province of Esmeraldas, aluminum and iron reached levels of 10 mg /L and 11 mg/L, respectively. In addition, values of 0.055 mg / L for chromium, 0.031 mg/L for nickel and 0.051 mg/L for zinc were obtained<sup>3</sup>.

The main industrial activities in the Province of Imbabura are related with the textile, leather tanning and mining industry, which are included in the most polluting industries<sup>4</sup>. These industries use large amounts of water that when discharged as wastewater contain a diversity of metal ions from cobalt, nickel, copper, lead, among others, which are toxic to living beings, even if they are found in very small amounts, because they are not biodegradable and tend to accumulate in the living organisms<sup>5</sup>. Several of the effects that these toxic metals show on humans and animals are of neurotoxic and carcinogenic nature<sup>6</sup>. Therefore, it is necessary to include, as a regular industrial activity, the evaluation of the quality of waste water to be discharged and to take the pertinent actions for decrease, and even eliminate, the harmful consequences.

**Table 1. Qualifying quality criteria for the preservation of flora and fauna in fresh, cold or warm waters, and in marine and estuary waters (Taken from: Norma de Calidad Ambiental y de Descarga de Efluentes: Recurso Agua<sup>1</sup>).**

Parameters	Units	Maximum Permissible Limit		
		Cold freshwater	Warm freshwater	Marine and estuary water
Cadmium (Cd)	mg/L	0.001	0.001	0.005
Copper (Cu)	mg/L	0.02	0.02	0.05
Cobalt (Co)	mg/L	0.2	0.2	0.2
Chrome (Cr)	mg/L	0.05	0.05	0.05
Tin (Sn)	mg/L			2.00
Iron (Fe)	mg/L	0.3	0.3	0.3
Mercury (Hg)	mg/L	0.0002	0.0002	0.0001
Nickel (Ni)	mg/L	0.025	0.025	0.1
Silver (Ag)	mg/L	0.01	0.01	0.005
Lead (Pb)	mg/L			0.01
Zinc (Zn)	mg/L	0.18	0.18	0.17

Unfortunately, in Ecuador only a small percentage of the waste generated by industrial activities receive a treatment and several of the final disposal methods used are not adequate, which implies a greater risk to health of human beings and implies a negative impact on the environment. In addition, Ecuador does not have adequate infrastructure or methods to assess the risks of the produced waste<sup>4</sup>.

Conventional processes to treat wastewater from industrial processes with presence of toxic metal traces include: membrane filtration, ion exchange, chemical precipitation, electrochemical treatment, and coagulation-flocculation<sup>7</sup>. Some of these processes involve a large investment of money and their results are not always efficient, as is the case of the elimination of metal ions when their concentrations are in the order of part per million (ppm). Also, several of these procedures need additional treatment, which generates an increase in the overall cost<sup>8</sup>. Compared to conventional processes, *Adsorption Method* is considered to be a convenient method for removing metals from water since it is an effective and low cost method with low environmental impact<sup>7</sup>.

## **2. PROBLEM STATEMENT:**

Some processes related to the textile and leather tanning industry and mining, which take place in the province of Imbabura, generate hazardous waste<sup>4</sup>, in which traces of some potentially toxic metal ions are found. The chemical species that are released must be eliminated from the residual effluents, since their presence represents a dangerous environmental impact and a harmful risk to the living beings. Conventional processes to address this problem include: membrane filtration, reverse osmosis, nanofiltration, ion exchange and chemical precipitation. These processes can be expensive and inefficient when working with very low concentrations of metals<sup>5</sup>. That is why the importance of low-cost and efficient non-convention techniques such as the use of adsorbents from biomass.

## **3. GENERAL AND SPECIFIC OBJECTIVES:**

### **3.1 General Objective**

Synthesis and evaluation of adsorbents prepared from biomass obtained from AW for heavy metal removal from industrial waste water originating from textile and leather tanning industry and mining.

### **3.2 Specific Objectives**

- Encourage interest in the development of adsorbents from biomass in order to increase the value of AW, fomenting the development of Green Chemistry.
- Use analytical spectroscopic (UV-Vis) and electrochemical methods (voltammetry) to determine the concentration of Ni<sup>2+</sup> and Co<sup>2+</sup> ions in solution subjected to the AP.
- Determine a model of metal ion adsorption with the use of adsorption isotherm models.
- Characterize the surface of the adsorbent before and after the AP through Raman and XPS techniques.

## 4. METHODOLOGY:

### 4.1 Reagents, Materials and Equipment

- **Reagents**

CoCl<sub>2</sub>\*6H<sub>2</sub>O (Sigma Aldrich, 98%), NiCl<sub>2</sub>\*6H<sub>2</sub>O (Sigma Aldrich, 98%), Distilled water, H<sub>2</sub>SO<sub>4</sub> (Sigma Aldrich, 98%), and Corn stalk from local sources (*Zea mays Amylacea*).

- **Materials**

Volumetric flask 50, 100 mL, Beakers 50 , 100 mL, Crisols, Kitasato 25 mL, Büchner funnel, Magnetic stir bar, Graduated pipettes 1, 2, 10 mL, Erlenmeyer flasks 50 mL, Storage bottles 20, 50 mL, Filter paper 4 micras, and Syringe filter 0.25 micras

- **Equipment**

Heating Magnetic Stirrer with Timer VELP SCIENTIFICA, Analytical Balance SAVAIN 152g/0.1mg HR-150A, Electrical oven POL-EKO APARATURA Temp.max.300°C, Electrical ginder DAEWOO DCG-362 Capacity: 50g 150W, UV/VIS/NIR/ Spectrometer Lambda 1050, AUTOLAB Potentiostat Galvanostat, LabRAM HR EVOLUTION RAMAN SPECTROMETER, and Scienta RS4000 photoemission system with cryo-manipulator (cools down to down to 20 K), monochromatic He I/He II UV and Al K $\alpha$  X-ray source

### 4.2 Theoretical Background

*Physical Adsorption* is presented by van der Waals attractive forces where the hydrogen bridges predominant that bind the adsorbate (specie to be adsorbed) on the surface of the adsorbent (solid on which the adsorbate is attracted). This process requires low temperature and suitable pH conditions. Also, this process presents a low heat of adsorption usually in the range of 10-40 kJ/mol. Nevertheless, *Chemical Adsorption* involves the presence of stronger interactions resulting from the chemical reactions that can occur between the adsorbent-adsorbate systems. As a result of these interactions, ionic and covalent bonds could be created. This process presents a high heat of adsorption usually in the range of 20-400 kJ/mol<sup>7,9</sup>.

In general, in the adsorption method there is a transfer of the metal ion of the solution towards the outer surface of the adsorbent, followed by a transport of mass by diffusion through the porous structure on the internal surface of the adsorbent. Finally, the adsorbate adsorption occurs on the active sites of the adsorbent pores<sup>10</sup>. In the case in which the adsorbent have not a porous structure, the AP is limited to the surface of the adsorbent. The AP is represented by means of *Isotherms of*

*Adsorption*, which are used to evaluate the interaction of ions or molecules constituents of the adsorbate with the surface of the adsorbent. These Isotherms are curves obtained from equations describing mathematically or the equilibrium state, established at constant temperature, between the amount of adsorbate in solution ( $C$ ) and the amount of adsorbate adsorbed on the adsorbent ( $\theta$ ) after a long enough contact. This dependence,  $\theta$  vs.  $C$ , can be derived theoretically (assuming the specific model of AP) or empirically (considering experimental data).

There exist several models of Isotherms of Adsorption, depending on the kind of mechanism described as well as the nature of the adsorbate and adsorbent involved. Nearly always, the amount adsorbed is normalized by the mass of the adsorbent to allow comparison of different materials. Maybe the most important model of these is given for the *Langmuir Isotherm*, however other models have given proposed, which are adopted by many studies<sup>11</sup>. In what follows are described briefly some of them.

### **Langmuir Isotherm**

It is a semi-empirical model derived from a proposed kinetic mechanism focused on a homogeneous AP, in which all of the active sites, where molecules would be adsorbed, have the same energy. Also, this model considers only the formation of a saturated monolayer, without consider the molecular interactions between molecules adsorbed<sup>11</sup>. The Langmuir model proposes equal adsorption and desorption rates of gases on solid surfaces, although it is also applicable to liquids<sup>12</sup>. The equation describing the Langmuir Isotherm is:

$$\theta = \frac{K_L C}{1 + K_L C} \quad (1)$$

where  $\theta$  is the equilibrium concentration of the amount of molecules adsorbed onto the solid phase,  $C$  is the equilibrium concentration of the fluid phase, and the  $K_L$  is the constant of adsorption equilibrium, an term related with the adsorption capacity.

### **Freundlich Isotherm**

It is an empirical model to represent the AP including the heterogeneity of the surface energy, and also considers the interaction between adsorbed molecules of the fluid phase<sup>13</sup>. The Freundlich equation represents the isothermal variation of the adsorption of a liquid or gas on the heterogeneous surface of a solid<sup>14</sup>. The equation associated with this model is:

$$\theta = K_F C^{\frac{1}{n}} \quad (2)$$

where  $\theta$  and  $C$  have the same mean as the Langmuir model, the equilibrium amount of molecules adsorbed on the solid and the equilibrium concentration of the fluid phase, respectively. The term  $K_F$ ,

known as Freundlich constant, is an indicator of the adsorption capacity, and  $n$  is a heterogeneity factor.

### Toth Isotherm

For a better description of heterogeneous systems it is proposed the Toth Isotherm, which is an empirical interpretation of the Langmuir model with slight variations in the terms, in order to improve the representation of system and to obtain a better fit of the experimental data<sup>13</sup>. In this model, an asymmetric Gaussian form is assumed for the distribution energy, especially for the sites that have an adsorption energy lower than the maximum<sup>11</sup>. The Toth Isotherm is represented by the equation:

$$\theta = \frac{C}{(K_T + (C)^n)^{\frac{1}{n}}} \quad (3)$$

Newly, the terms  $\theta$  and  $C$  have the same mean given in previous models,  $n$  represents the system heterogeneity ( $0 < 1/n < 1$ ) and  $K_T$  is a constant associated with the affinity of interaction.

### Sips Isotherm

It is a representation that combines the Langmuir and Freundlich Isotherms. This model is associated with adsorption on heterogeneous surfaces. For low concentrations of adsorbate the Sips isotherm is reduced to the Freundlich model, and at high concentrations the Langmuir model is obtained, this is because the AP can be represented by a monolayer formation<sup>13</sup>.

$$\theta = \frac{K_s C^{\frac{1}{n}}}{1 + K_s C^{\frac{1}{n}}} \quad (4)$$

where the terms  $\theta$ ,  $C$  and  $n$  have the same mean given in previous models, and  $K_s$  is the affinity constant of this model.

### Bio-sorption method

Particularly, when the adsorbent is prepared from natural sources or agriculture waste, giving a focus mainly to the stem, bagasse, and straw of corn, sugar cane, flowers, wheat, cotton, and other vegetal material; the resultant material is called *bio-adsorbent*. The bio-sorption method has achieved great success, in relation to conventional processes, because of the advantage that the adsorbent is obtained from inexpensive and highly available materials as well as for its high effectivity for trapping metal ions, even for low metal concentration in wastewater in the order of *ppm* to *ppb* levels in aqueous solutions<sup>8,10</sup>. Once the metal ion is attached to adsorbent, the metal bio-sorption occurs, leading to an uptake of metal, or metal ions, by the active sites of the solid adsorbent through an attractive physical interactions, ion exchange, and/or chemical bonds<sup>15,16</sup>.

The responsible of the trapping of metal ions by the bio-adsorbent is the *Biomass* of the vegetal sources, which is principally composed of cellulose, lignin and hemicellulose. Although the most abundant constituent is the cellulose, has been proposed that the lignin is the constituent with a greater effectivity for metals trapping<sup>17,18</sup>. Lignin is a natural polymer located in the cell walls of plants, occurring in large quantities<sup>17</sup>. The structure of lignin consists of aromatic rings which form a large number of hydrogen bonds and the presence of phenolic compounds and labile methoxy groups<sup>18</sup>. In addition, it presents polar groups such as alcohols, aldehydes, ketones, carboxylic groups and ethers (Figure 1)<sup>19</sup>.

The presence of carboxylic and phenolic groups in the lignin exhibits a greater affinity with metals, which explains the high capacity of adsorption by lignin<sup>20</sup>. It is believed that the method of uptake of metal ions by lignin occurs by the binding of metal ions through these functional groups of lignin<sup>21</sup>. Although a specific mechanism has not been established to explain the process of metal adsorption on lignin, it is thought that this mechanism involves processes such as ion exchange, surface adsorption and complexation<sup>17</sup>.

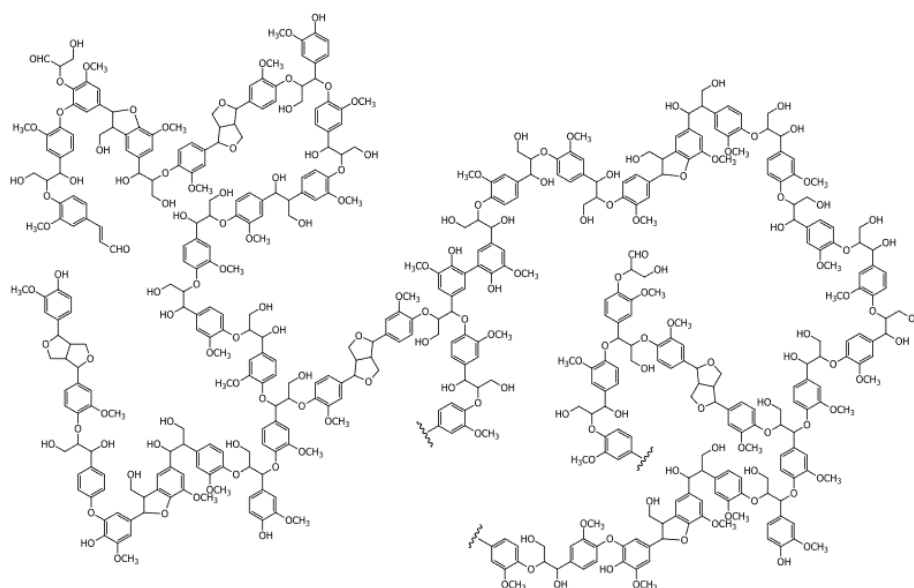


**Figure 1. Chemical structure of lignin proposed by Chavez for the extract of plant species. Taken from Chávez<sup>19</sup>.**

### 4.3 Experimental Procedure A - Adsorption Process Stage.

#### 4.3.1 Adsorbent preparation:

The AW used in this project was *Corn stalk*, which was obtained from a local crops of the Province of Imbabura, where exist large areas of corn cultivation and few alternatives are used for harness it, different to be used as compost. Therefore it is proposed to recover this kind of waste and from it to prepare an adsorbent material with the ability to potentially remove toxic metal present in aqueous solutions. For doing this, a procedure was followed for the preparation of adsorbent that consisted of the washing of the small pieces of the corn stalk with distilled water, that then were dried to 50°C overnight for remove the water from the sample preparation process, and milled using an electrical grinder. Once obtained the finely diluted solid, washed and grinded, it was incinerated to 300°C for three hours. Solid is transformed into a type of coal that only contains lignin structure, eliminated other components present in the biomass. Lignin, unlike cellulose and hemicellulose, decomposes more slowly, over a wider temperature range (200-500°C)<sup>22</sup>, and then it was storage for its further use.

#### 4.3.2 Solution preparation:

Stock solutions of Co<sup>+2</sup> and Ni<sup>+2</sup> are prepared by dissolving a certain amount the respective salt in distilled water, and then diluting until the objective concentrations.

**NiCl<sub>2</sub> 0.1 M:** 2.3778 g of NiCl<sub>2</sub>\*6H<sub>2</sub>O were dissolved with 100 mL of distilled water.

From this stock solution was prepared a set of solutions of Ni<sup>2+</sup> between 1x10<sup>-1</sup> M and 1x10<sup>-3</sup> M.

**CoCl<sub>2</sub> 0.1 M:** 2.3794 of CoCl<sub>2</sub>\*6H<sub>2</sub>O were dissolved with 100 ml of distilled water.

From this stock solution was prepared a series of solutions of Co<sup>+2</sup> in the range of 1x10<sup>-1</sup>M – 1x10<sup>-3</sup>M.

#### 4.3.3 Adsorption process:

The adsorption experiments were carried out pouring 0.1 g of prepared adsorbent in a 50 mL beaker and mixed with 10 ml of metal ion solutions, during this process was kept stirring for 45 minutes with a magnetic stir bar. At the end of the stir the sample was left to rest for 5 minutes. The solution was separated from the adsorbent by vacuum filtration with a filter paper with a pore size of 4 µm, recording the initial and final weight of the solid involved. All the experiments were carried out at room temperature. In some cases were used different mass of adsorbent, but the V<sub>solution</sub>: m<sub>adsorbent</sub> proportion remained constant at 10:0.1 (v/w). A schematic diagram of the procedure is shown in the Figure 2.

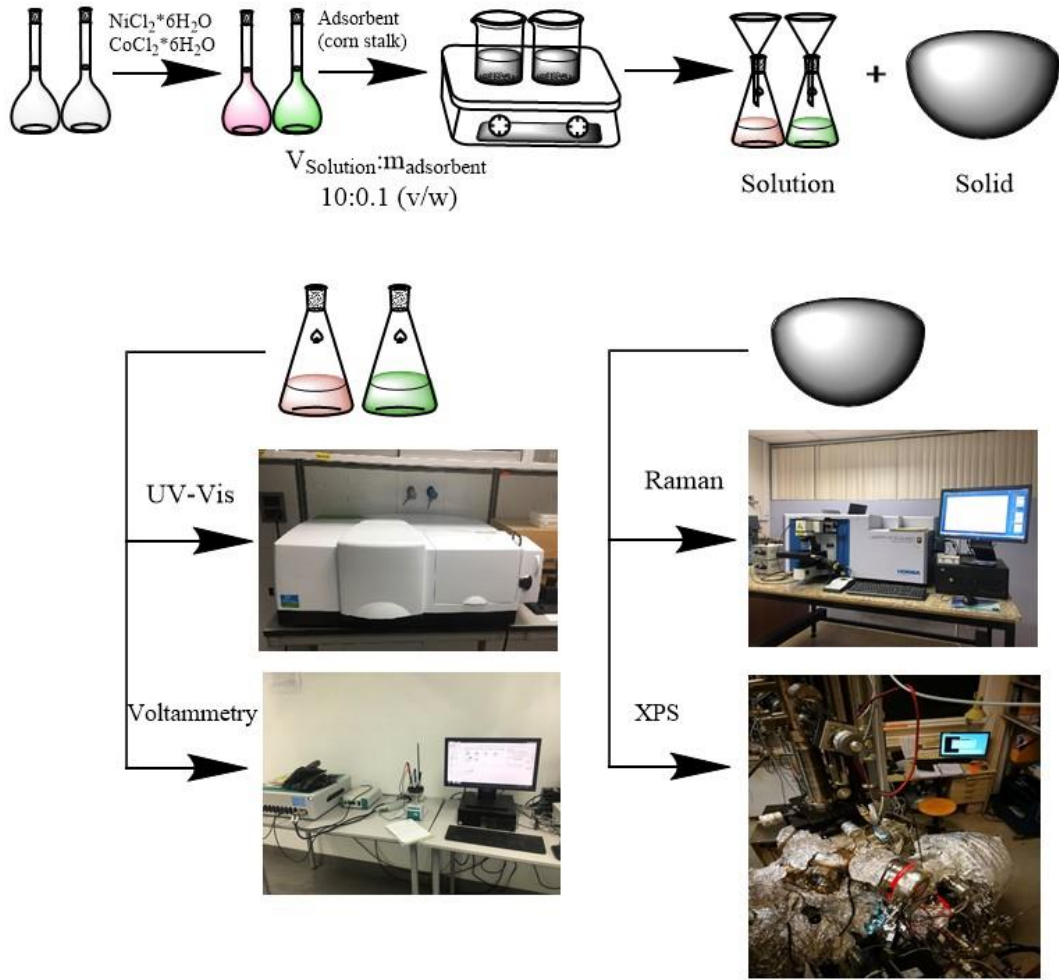


**Figure 2. Scheme of Adsorption Process Stage.**

The amount of adsorbed was calculated from the loss of moles of the metal ions in solution during of the AP, by the equation 5, taking into account the volume of the sample. The different values obtained are shown in the Table 6, Table 7, Table 8 and Table 9.

$$Adsorbed_{Amount} = ([Metal^{2+}]_{Initial} - [Metal^{2+}]_{Final}) * V_{solution} \quad (5)$$

It is convenient to express the capacity of the adsorbent to removal metal ions from solutions as a specific quantity, that is, adsorbed amount per gram of adsorbent ( $Adsorbed_{Amount-gads}$ ), which is calculated from:

$$Adsorbed_{Amount-gads} = \frac{Adsorbed_{mol}}{Adsorbed\ mass} \quad (6)$$

#### 4.4 Experimental Procedure B - Solution Characterization Stage.

For the measurements of the amount of adsorbed metal ions it was required to recorded the concentration of these metal ions before and after of the AP. These concentration were determined using spectroscopic and voltammetry methods. Although the desired range of concentration, that is, estimated values to be found in the residual water wastes, is lower than that evaluated in this project,

the equipment infrastructure currently available in the Laboratory of Chemistry did not allow to explore this desired range of concentrations. However, the evaluation of the capacity of removal of metal ions by adsorbents prepared, and the AP involved, can be analyzed for the range of concentrations studied.

#### 4.4.1. UV-Visible Spectroscopy.

UV-Visible spectroscopy was used to measure the absorbance of ultraviolet or visible light by a sample. A light source generates a visible and near ultraviolet radiation that covers a range of 200 - 800 nm, the light output is then focused on the diffraction grating that causes a division of the light that enters its component colors of different wavelengths. In a liquid sample, the intensity of light passing through the sample and the blank (solvent in which the sample is dissolved) for each wavelength is measured. The result of UV-Visible spectroscopy is given as a graph of absorbance ( $A$ ) given in arbitrary units (a.u.) versus wavelength ( $\lambda$ ) given in nanometers (nm)<sup>23</sup>.

The UV-Vis is based on the *Beer-Lambert Law*, which states that the absorbance is proportional to the concentration. Beer-Lambert Law is represented by the equation:

$$A = \epsilon cl \quad (7)$$

where  $A$  is the absorbance (a.u.),  $\epsilon$  is molar extinction coefficient ( $M^{-1} \text{ cm}^{-1}$ ),  $c$  is the concentration (M), and  $l$  is the path length (cm).

The equipment used for the UV-Vis measurements in this project was an UV / VIS / NIR / Spectrometer Lambda 1050, working in the visible range of 200-800 nm. A blank of distilled water was used for the all measurement of the samples. The concentrations range evaluated of the metal ions  $\text{Ni}^{2+}$  and  $\text{Co}^{2+}$  was  $1 \times 10^{-1} \text{ M} - 1 \times 10^{-3} \text{ M}$  for both cases.

#### 4.4.2. Voltammetry.

For the voltammetry measurements was used the equipment AUTOLAB Potentiostat Galvanostat, using a platinum electrode as the working electrode, and a current range of 1mA was used for the linear sweep voltammetry. In general, for the cobalt and nickel solutions a maximum potential value ( $E_p$ ) is observed in a potential range of 0.6-1.8V, the concentration range of evaluated solutions was  $1 \times 10^{-1} \text{ M} - 1 \times 10^{-3} \text{ M}$ .

The voltammetry equipment, shown in the Figure 3, consists of a cell and three electrodes:

- Working electrode in which the reaction occurs. Initially was tested a glass carbon electrode, but for the case of cobalt solutions evaluation it was not convenient. Therefore, it was decided to use the *Pt disc RRDE* electrode tip of 5 mm.

- Reference electrode with a known potential. Silver / silver chloride reference electrode with  $c(\text{KCl}) = 3 \text{ mol/L}$ .
- A Pt wire was used as a counter electrode.

The procedure developed for the voltammetry technique consisted in recording the current that is generated for a given potential of certain samples<sup>24</sup>. It was added to each solution evaluated a known amount of concentrated  $\text{H}_2\text{SO}_4$  until reaches a concentration of 1 M to assure an increase of the conductivity of solution.

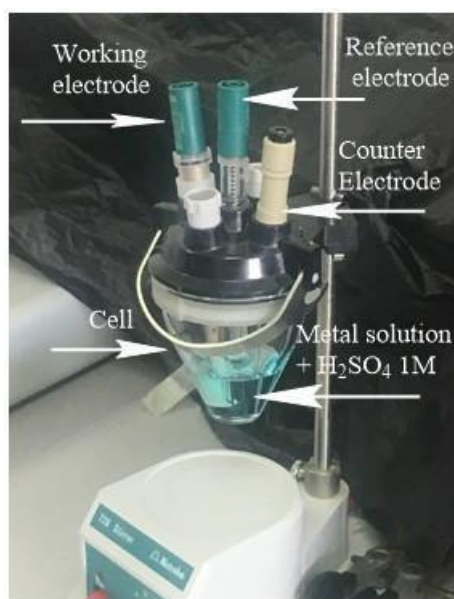


*Figure 3. Electrochemical cell for voltammetry experiments.*

#### 4.2.2.1 Cyclic voltammetry

The potential creates a wave increasing the current to a maximum point ( $E_p^{\text{red}}$ ), then as the potential reverses an oxidation current is observed ( $E_p^{\text{ox}}$ ). The potential present in the electrode causes the sample to oxidize or reduce. This technique allows to create a potential window in order to establish the oxidation of the anion and the reduction of the cation<sup>25</sup>. Such potential window is the input for the linear sweep voltammetry technique.

#### 4.2.2.2 Linear sweep voltammetry

A sweep is performed applying a potential, then the current flowing in the system is transformed into voltage. The features of interest for this method are the peak current ( $I_p$ ), and the peak potential ( $E_p$ ). An initial and an end potential is used for the reaction of interest<sup>25</sup>. From this technique were obtained the conductivity curves, in which is plotted current vs potential, that is I-V curves. The maximum of each these curves is taken as the current associated to the solution with its respective concentration.

In a planar diffusion the peak current is given by the Randles-Sevcik equation, which at 25°C can be described as:

$$I_p = (2.69 \times 10^5) n^{\frac{3}{2}} A D_o^{\frac{1}{2}} C_o^* v^{\frac{1}{2}} \quad (8)$$

where  $I_p$  is the current peak (in A),  $A$  is the electrode area (in cm<sup>2</sup>),  $D_o$  diffusion coefficient (in cm<sup>2</sup>/s),  $C_o^*$  is the concentration (in mol/cm<sup>3</sup>), and  $v$  is the sweep rate (in V/s). Equation 8 states that the peak current is proportional to the square roots of scan rate ( $v^{1/2}$ )<sup>26</sup>.

## 4.5 Experimental Procedure C - Solid Characterization Stage.

### 4.5.1 X-ray Photoelectron Spectroscopy (XPS)

The technique consists of to lead the photons from the radiation of soft X-rays to a sample in an ultra-high vacuum, analyzing the photoelectrons emitted from the sample in relation to the kinetic energy. This technique analyzes the chemical composition of the surface of the material up to a depth of a few nm<sup>27</sup>.

In the XPS spectrum of graphitic materials it is important to analyze the C1s and O1s lines in order to obtain information about the spectrum such as the chemical states present in the sample, as well as the calibration of the energy scale or a reference, this because the measured signals as well as the position of the C1s must be calibrated from a reference<sup>28,29</sup>.

To interpret the peaks obtained in the XPS spectrum, the *Binding Energy* values found in the literature are used. However, the data obtained is in *Kinetic Energy*, which is why this data is converted using the equation 9 to binding energy in order to analyze the data obtained.

$$Binding\ Energy = 1486.7 - 4.77 - Kinetic\ Energy \quad (9)$$

The measurements by this technique were developed thanks to the collaboration of Juan Carlos Moreno Ph.D., currently working at *Materials Laboratory of Austrian University*. The equipment used was a Scienta RS4000 photoemission system with cryo-manipulator (cools down to down to 20 K), monochromatic He I/He II UV and Al K $\alpha$  X-ray source.

#### 4.5.2 Raman spectroscopy (RaS)

The mechanism of the Raman dispersion is based on the change of the quantum states of rotation or vibration of the molecules. The greater part of light scattering that is generated in a sample is the *Rayleigh scattering* that corresponds to an elastic dispersion without loss of energy and without frequency change. However, Raman works with the inelastic scattering of the incident photons that generate a change in energy due to changes in the vibrational or rotational modes of the molecules present in the sample<sup>30</sup>.

Raman shifted photons that exhibit low energy are known as *Stokes scattering* while those with higher energies than the Rayleigh elastic line are known as *anti-Stokes scattering*. The intensity of the lines is proportional to  $(n + 1)$  for Stokes scattering and proportional to  $n$  for anti-Stokes scattering, where  $n$  is the occupation number of the phonon. As a result, the Stokes line is more intense compared to the anti-Stokes line. Generally only the Stokes spectrum is registered for analysis in Raman spectroscopy<sup>31</sup>. The measurements were carried out in the *Laboratorio de Nuevos Materiales of Escuela Politécnica Nacional*, who are collaborators of the project. The equipment used was a LabRAM HR EVOLUTION RAMAN SPECTROMETER.

## 5. RESULTS, INTERPRETATION AND DISCUSSION:

### 5.1 Preparation of calibration curves:

The concentration data obtained from the measurements by UV-Vis spectroscopy and Voltammetry methods for the different solutions allowed the construction of the CC for each species evaluated. The resulting equations of the linear fit of the CC for each metal ion solution are shown in the Table 3 and Table 5 showing the data obtained by both methods used, that is, by UV-Vis spectroscopic and voltammetry methods.

### UV-Vis Spectroscopic measurements.

As was mentioned above, the evaluated concentrations range of metal ions solutions was from  $1 \times 10^{-1}$  M to  $1 \times 10^{-3}$  M. The spectra obtained are shown in Figure 5-(a) for the nickel solutions and in Figure 5-(b) for the cobalt solutions. The bands observed are due to the complex formed between the metal ions,  $\text{Ni}^{2+}$  and  $\text{Co}^{2+}$ , with the water in the medium, which are represented in Figure 6-(a) and Figure 6-(b), respectively.

It is shown the formation of an octahedral structure of  $\text{Ni}^{+2}$  linked to 6 water molecules for the first coordination layer,  $[\text{Ni}(\text{H}_2\text{O})_6]^{2+}$ , taking into account the electronic configuration  $d^8$  of high spin<sup>32</sup>, for the ground state ( $^3\text{A}_{2g}$ ) of the Ni ion in an octahedral field, three allowed transitions are presented. The first transition corresponding to  $^3\text{T}_{2g} \leftarrow ^3\text{A}_{2g}$  is not recorded because it is located in the infrared region. The second transition is  $^3\text{T}_{1g}(\text{F}) \leftarrow ^3\text{A}_{2g}$  is located in the range 800-550 nm, it is observe a peak at 722 nm and a shoulder at 658 nm, and this is given by the spin orbit coupling that produces a mixture of  $^3\text{T}_{1g}(\text{F})$  and  $1\text{E}_g$  states. The last transition corresponds to  $^3\text{T}_{1g}(\text{P}) \leftarrow ^3\text{A}_{2g}$  for the range ~500-350 nm. This band has the highest intensity because this transition is proportional to  $(10Dq)^{33}$ .

On the other hand, the cobalt ion forms an octahedral complex  $[\text{Co}(\text{H}_2\text{O})_6]^{2+}$ , taking into account the electronic configuration  $d^7$  of high spin, for the ground state ( $^4\text{T}_{1g}(\text{F})$ ) of the Co ion in an octahedral field, three allowed transitions are presented. The first band is located in the infrared region which corresponds to the transition  $^4\text{T}_{2g} \leftarrow ^4\text{T}_{1g}(\text{F})$ . The second transition located around 625-642 nm corresponds to  $^4\text{A}_{2g} \leftarrow ^4\text{T}_{1g}(\text{F})$ , which appears with a very small intensity. The band that is observed around 500 nm corresponds to the transition  $^4\text{T}_{1g}(\text{P}) \leftarrow ^4\text{T}_{1g}(\text{F})$ . The spectral shoulder appears in the short wavelengths of the absorption spectrum because of the spin-orbit interaction in the excited state  $^4\text{T}_{1g}(\text{P})$ <sup>32,34,35</sup>.

The transitions corresponding to the signals of UV-Vis for nickel and cobalt solution are represented in Figure 4.

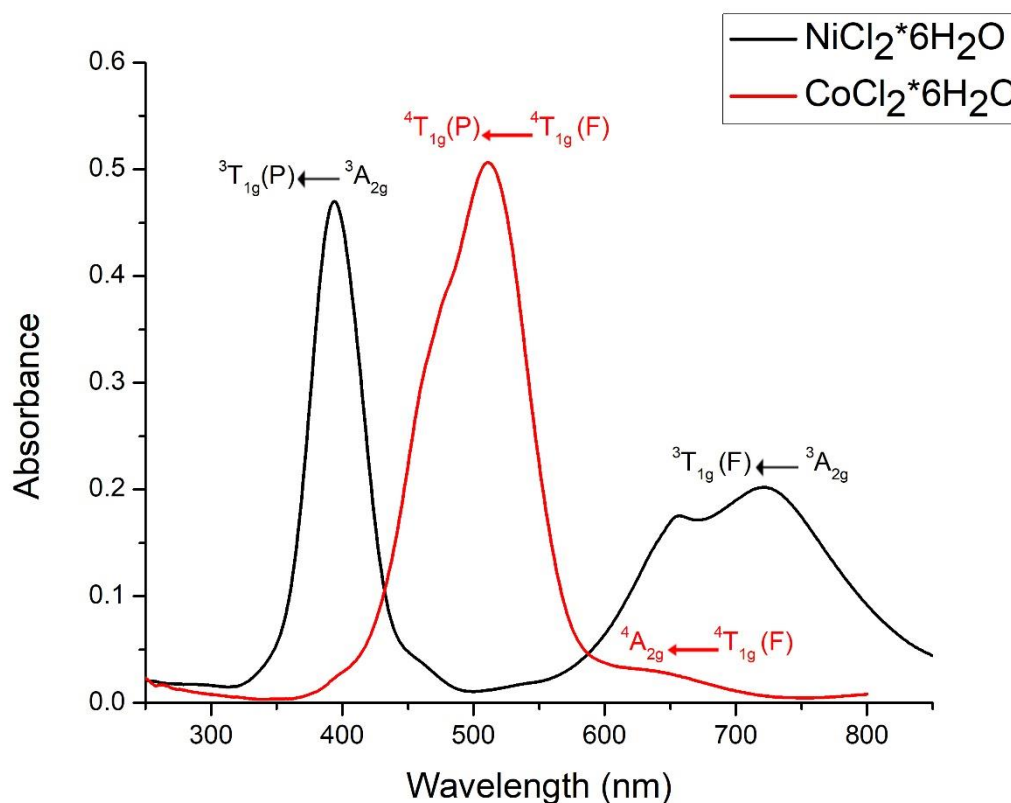


Figure 4. Transitions of the signals of UV-Vis for nickel and cobalt solution.

In the Figure 5-(a) and Figure 5-(b) it can be seen that the signal in the spectra of both nickel and cobalt decreases, until the concentration reaches values in the millimolar order, for which the signal is lost. Unfortunately, using only as references the metal complexes formed with water it is not possible to reach lower concentrations without ambiguity. However, because the proposal is evaluate the capacity of the solid prepared to remove the mentioned metal ions, the chosen range allow to monitoring this evaluation.

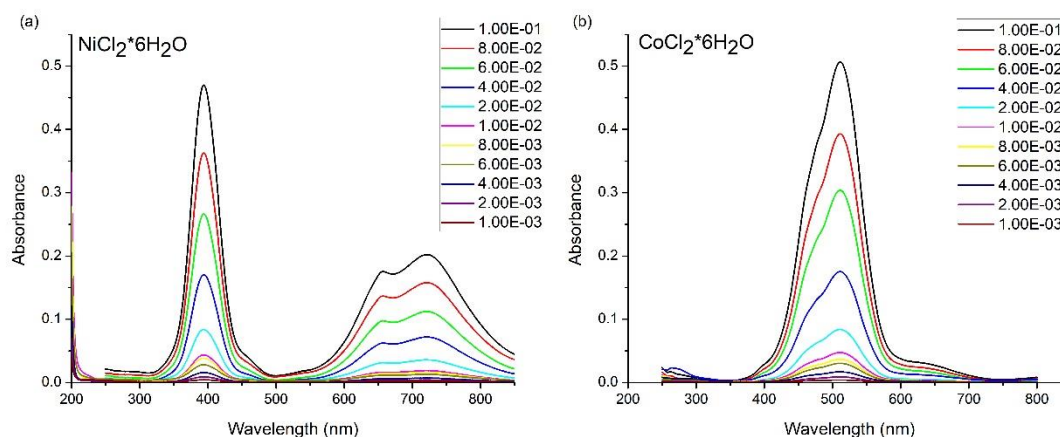
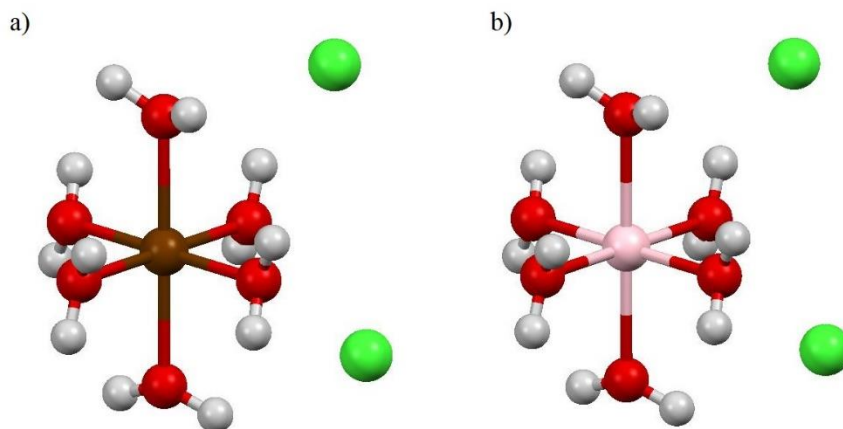


Figure 5. Obtained spectra from measurements of UV-Vis spectroscopy for evaluated (a) Nickel solutions and (b) Cobalt solutions.



*Figure 6. Representation of (a)  $[\text{Ni}(\text{H}_2\text{O})_6]\text{Cl}_2$  and (b)  $[\text{Co}(\text{H}_2\text{O})_6]\text{Cl}_2$ . Atoms are represented as spheres with conventional color coding: nickel (brown), cobalt (pink), oxygen (red), hydrogen (white), and chlorine (green).*

For the nickel solutions spectrum, from the absorbance for the peak appearing at the wavelength of  $\sim 720$  nm the CC was constructed, this due there is an overlap of peaks as evidenced later in Figure 12, the sensitivity of the equipment does not allow to measure low concentrations of metal ion solutions, so it is believed that the loss of the peak at 400nm is due to the fact that the equipment noise begins to take on significance and interferes with the absorbance signal. For cobalt solutions was used the values of absorbance for the peak occurring at the wavelength of  $\sim 510$  nm.

The CC for the absorbance of  $\text{Ni}^{2+}$  and  $\text{Co}^{2+}$  solutions are shown in Figure 7-(a) and Figure 7-(b), respectively, which were constructed using the values given in Table 2 for the nickel case and in Table 4 for the cobalt case. It can be seen that good linear fits were obtained, and the resulting equations for the respective fits are given in Table 3 for the nickel solutions and in Table 5 for the cobalt solutions. From these equations the concentration values for the nickel and cobalt solutions were calculated, represented in the Table 2 and Table 4 by  $[\text{Ni}^{2+}]_{\text{Fit-UV}}$  and  $[\text{Co}^{2+}]_{\text{Fit-UV}}$ , respectively. These concentration values obtained was used as the initial values to considered in the AP, from which were compared the amounts of free metal ions in solutions.

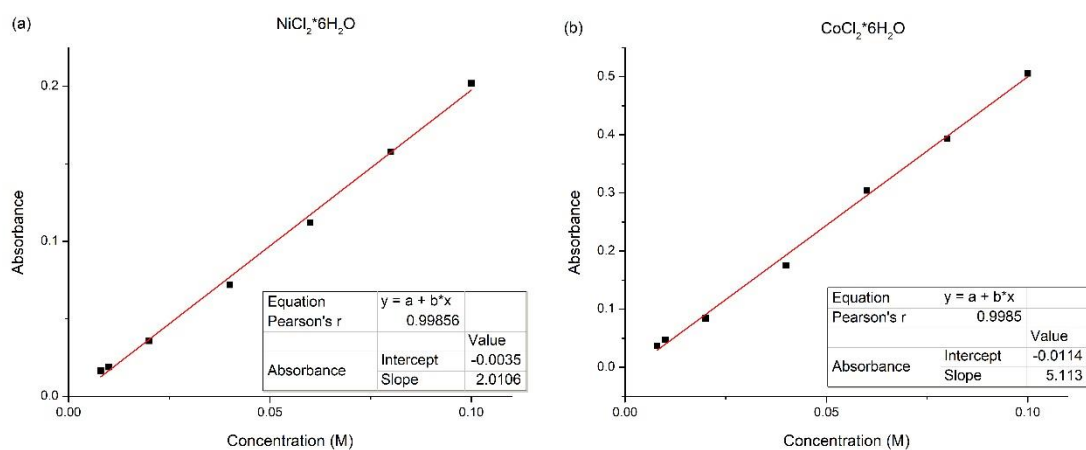


Figure 7. Calibration curves obtained from Absorbance measured in the UV-Vis spectrometer for (a)  $\text{NiCl}_2 \cdot 6\text{H}_2\text{O}$  solutions ( $\sim 720 \text{ nm}$ ) and (b)  $\text{CoCl}_2 \cdot 6\text{H}_2\text{O}$  solutions ( $\sim 510 \text{ nm}$ ).

From values of regression coefficients obtained, which are shown together with the linear fit equations, the CC for the absorbance of the nickel and cobalt solutions are satisfactory.

### Voltammetry measurements.

The determination of metal ions concentrations was also carried out by voltammetry measurements of the solutions prepared. The chosen concentration range was the same for the UV-Vis spectroscopic measurements, but with the difference that was added concentrated  $\text{H}_2\text{SO}_4$  to the solutions, the function of the supporting electrolyte is to avoid the distortion of the oxidation peaks; the same amount for all of them, with the proposal of increase the conductivity of the evaluated solutions. In general, for the concentration range evaluated for the nickel and cobalt solutions ( $1 \times 10^{-1} \text{ M} - 1 \times 10^{-3} \text{ M}$ ) the working conditions were established: scan rate  $0.01 \text{ mVs}$ , # scans 3, and stop potential  $0.8$ . The process was carried out at room temperature. The values for the potential, denoted by  $E_p$ , were observed in a potential range of  $0.6$ - $1.8 \text{ V}$ .

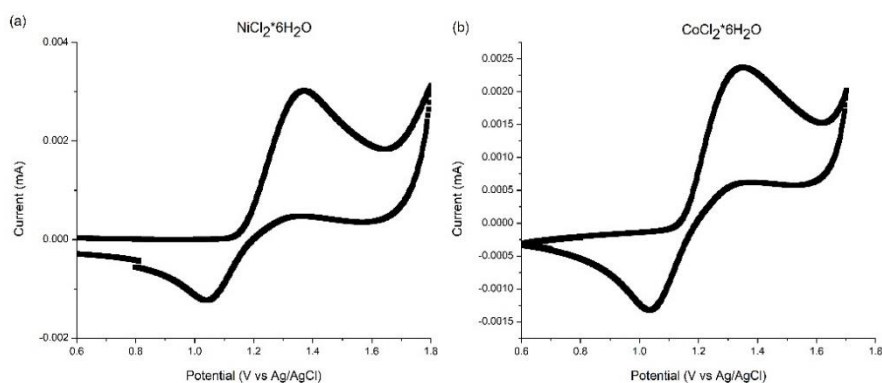
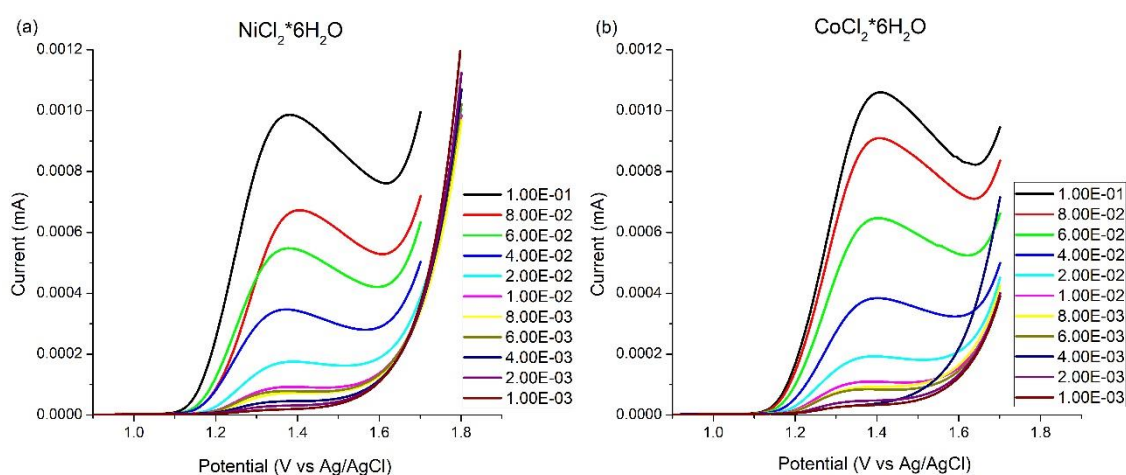


Figure 8. Cyclic voltammogram for (a)  $\text{NiCl}_2 \cdot 6\text{H}_2\text{O}$  solution and (b)  $\text{CoCl}_2 \cdot 6\text{H}_2\text{O}$  solutions.

The cyclic voltammogram of nickel solution (Figure 8-(a)) shown a broad reduction peak  $\sim 1.05$  V which is attributed to the reduction of  $\text{Ni}^{+2}$  to Ni metal and a broad oxidation peak  $\sim 1.4$  V<sup>36</sup>. Cyclic voltammogram of cobalt solution (Figure 8-(b)) presents the same conditions as the nickel solution.

The determination of maximum of current of solutions was directly measured, observing the expected behavior, the higher concentration the higher peak current, which are shown in the Figure 9-(a) for the nickel and in Figure 9-(b) for the cobalt. The obtained values are shown in the Table 2 and Table 4 for the nickel and cobalt solutions, respectively, and they were used for the construction of the CC for the current for the metal ions. The resulting equations are given in the Table 3 and Table 5, denoting the concentration to be calculated as  $[\text{Ni}^{2+}]_{\text{Fit-Volt}}$  and  $[\text{Co}^{2+}]_{\text{Fit-Volt}}$ , for each case.



**Figure 9.** Current curves obtained from Voltammetry measurements for (a)  $\text{NiCl}_2 \cdot 6\text{H}_2\text{O}$  solutions and (b)  $\text{CoCl}_2 \cdot 6\text{H}_2\text{O}$  solutions.

This voltammetry method results more sensitive, and it could be possible to access lower concentration than  $1 \times 10^{-3}$  M. However, the concentration range was kept to that initially chosen to evaluate the capacity of the adsorbent.

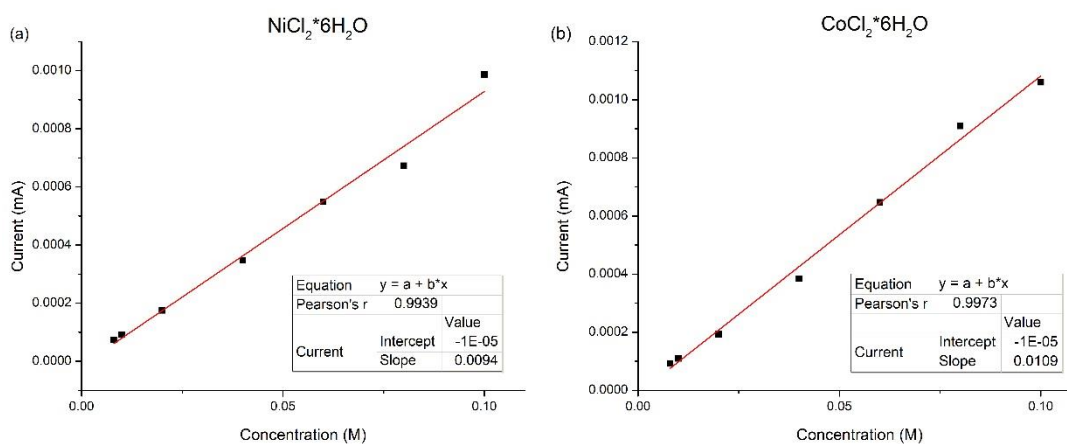


**Figure 10.** Calibration curves for current measurements from voltammetry methods for (a)  $\text{NiCl}_2 \cdot 6\text{H}_2\text{O}$  solutions and (b)  $\text{CoCl}_2 \cdot 6\text{H}_2\text{O}$  solutions.

From the CC for the current of nickel and cobalt solutions (Figure 10) the values of regression coefficients were obtained, which are shown together with the linear fit equations and these are satisfactory.

**Table 2.** Values of the absorbance by UV-Vis measurements (at ~720 nm) and the current (in mA) for  $\text{Ni}^{2+}$  solutions

$[\text{Ni}^{2+}]_0$ (M)	Abs (700 nm)	$[\text{Ni}^{2+}]_{\text{Fit-UV}}$ (M)	Current (mA)	$[\text{Ni}^{2+}]_{\text{Fit-Volt}}$ (M)
1.00E-01	0.2019	0.102159	0.000987	0.106064
8.00E-02	0.1577	0.080175	0.000673	0.072660
6.00E-02	0.1122	0.057545	0.000548	0.059362
4.00E-02	0.0719	0.037501	0.000347	0.037979
2.00E-02	0.0358	0.019546	0.000175	0.019681
1.00E-02	0.0189	0.011141	9.25E-05	0.010904
8.00E-03	0.0165	0.009947	7.3E-05	0.008830

The equation for the CC for the nickel solution, for UV-Vis and voltammetry measurements, as well as their regression coefficients (R), are shown in Table 3.

**Table 3.** Fit Equations obtained for UV-Vis and Voltammetry for  $\text{Ni}^{2+}$  solutions.

$\text{Absorbance} = 2.0106[\text{Ni}^{2+}] - 0.0035$ $R = 0.9986$	$\text{Current} = 0.0094[\text{Ni}^{2+}] - 0.00001$ $R = 0.9939$
$[\text{Ni}^{2+}]_{\text{Fit-UV}} = \frac{\text{Absorbance} + 0.0035}{2.0106}$	$[\text{Ni}^{2+}]_{\text{Fit-Volt}} = \frac{\text{Current} + 0.00001}{0.0094}$

The same evaluation was developed for the cobalt solutions, and the data and results for the respective fits are shown in the Table 4 and Table 5.

**Table 4. Values of the absorbance by UV-Vis measurements (at ~510 nm) and the Current (in mA) for Co<sup>2+</sup> solutions.**

[Co <sup>2+</sup> ] <sub>0</sub> (M)	Abs (510 nm)	[Co <sup>2+</sup> ] <sub>Fit-UV</sub> (M)	Current (mA)	[Co <sup>2+</sup> ] <sub>Fit-Volt</sub> (M)
1.00E-01	0.5056	0.101115	0.001060	0.098182
8.00E-02	0.3929	0.079073	0.000910	0.084379
6.00E-02	0.3039	0.061666	0.000647	0.060273
4.00E-02	0.1753	0.036515	0.000384	0.036130
2.00E-02	0.0839	0.018639	0.000193	0.018609
1.00E-02	0.0474	0.011500	0.000110	0.010974
8.00E-03	0.0368	0.009427	0.000093	0.009446

**Table 5. Fit Equations obtained for UV-Vis and Voltammetry for Co<sup>2+</sup> solutions**

$\text{Absorbance} = 5.113[\text{Co}^{2+}] - 0.0114$ $R = 0.9985$	$\text{Current} = 0.0109[\text{Co}^{2+}] - 0.00001$ $R = 0.9973$
$[\text{Co}^{2+}]_{\text{Fit-UV}} = \frac{\text{Absorbance} + 0.0114}{5.113}$	$[\text{Co}^{2+}]_{\text{Fit-Volt}} = \frac{\text{Current} - 0.00001}{0.0109}$

## 5.2 Measurements of [Ni<sup>2+</sup>] by UV-Spectroscopy and Voltammetry after of the Adsorption Process:

Using the equations of CC fits, by both methods, the concentrations of nickel ion remaining in solutions were determined from the corresponding values for the absorbance and current for the solutions evaluated. These values are given in the Table 6 and Table 7, respectively. The term  $[Ni^{2+}]_{Initial}$  it is referred to the value of concentration of nickel ion in solution before the AP, calculated from equation of the CC for the absorbance of nickel solution for the Table 6 case, and from equation of the CC for the current of nickel solution for the Table 7 case. The term  $[Ni^{2+}]_{Final}$  corresponds to the value of concentration calculated for the nickel solutions after the AP.

It is important to mention that for the solutions with the two lowest values of nickel concentration was required to filter the solutions with a syringe filter with a pore size of 0.22  $\mu m$ , because the values of current resulted higher than that of initial concentration ( $[Ni^{2+}]_{Initial}$ ). These solutions presented a change of color, from light green to light brown, as it is shown in the Figure 11-(a) and Figure 11-(b). Possibly, the coloration exhibited is due to the formation of very small hydro-soluble carbonaceous structures with a capacity to interact with nickel, complexing it or reducing it. Once filtration was made, the conductivity measurements of resulting solution were consistent with the concentration of solutions previously measured. Unfortunately, a more appropriate characterization, for example by Transmission Electron Microscopy, to demonstrate the presence of these carbonaceous structures in solution could not be used. It would have been a good option.

Once the AP was finished, as described in section 4.3.3, it was recorded the absorbance for the resulting solution. The equation 5 was used to determine the amount of adsorbed moles (in the tables denoted as *Adsorbed Amount*), and by the equation 6 was calculated the adsorbed amount per gram of adsorbent (in the tables denoted as *Adsorbed Amount / g<sub>ads</sub>*). Finally, the capacity for removal of the metal ions from solutions was evaluated by the adsorption percent calculated (in the tables denoted as *% Adsorption*).

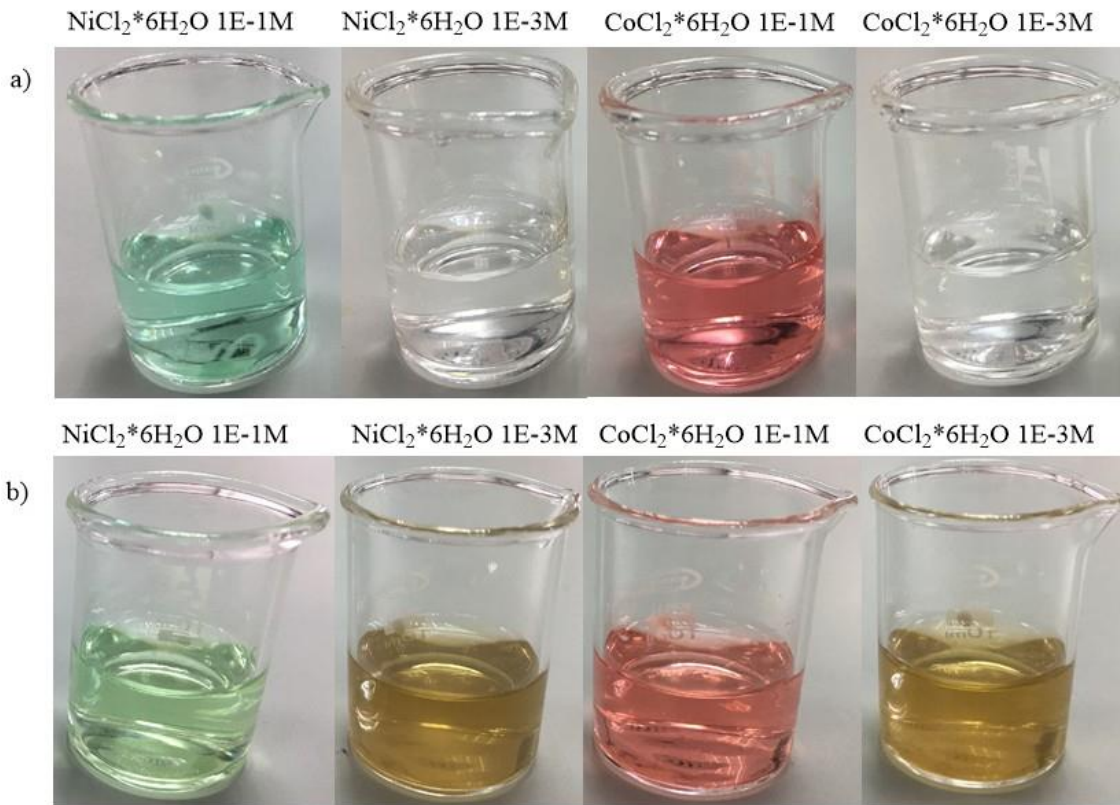


**Figure 11.** Pictures of samples of the solutions evaluated, (a) before and (b) after of adsorption process for Nickel and Cobalt solutions.

After the AP, the decrease in absorbance between Figure 5 (for solutions before AP) and Figure 12 (for solutions after AP), it was evident for both nickel and cobalt solutions. In addition, a decrease in current could be observed for nickel and cobalt solutions between Figure 9 (for solutions before AP) and Figure 13 (for solutions after AP).

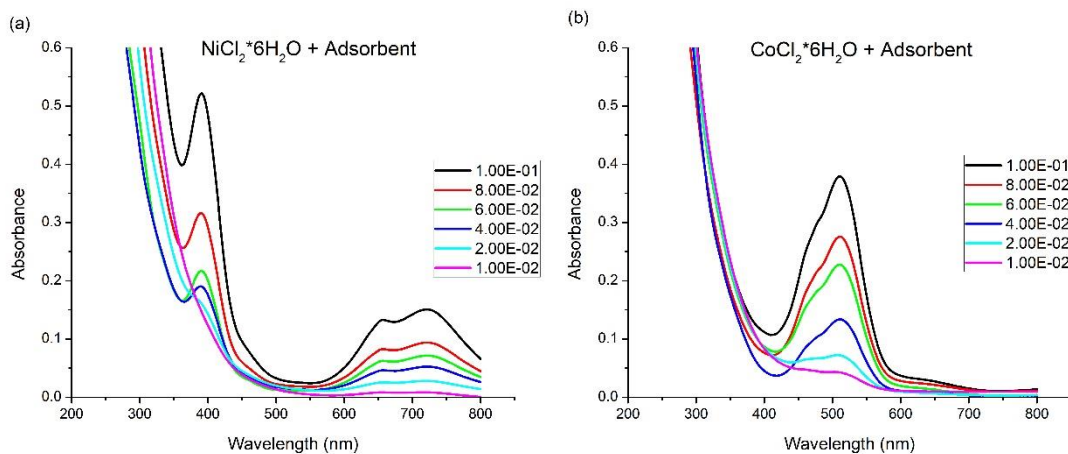


**Figure 12.** Absorbance graph (a)  $\text{NiCl}_2 \cdot 6\text{H}_2\text{O}$  solution (722nm) and (b)  $\text{CoCl}_2 \cdot 6\text{H}_2\text{O}$  solution (510 nm) after of adsorption process.

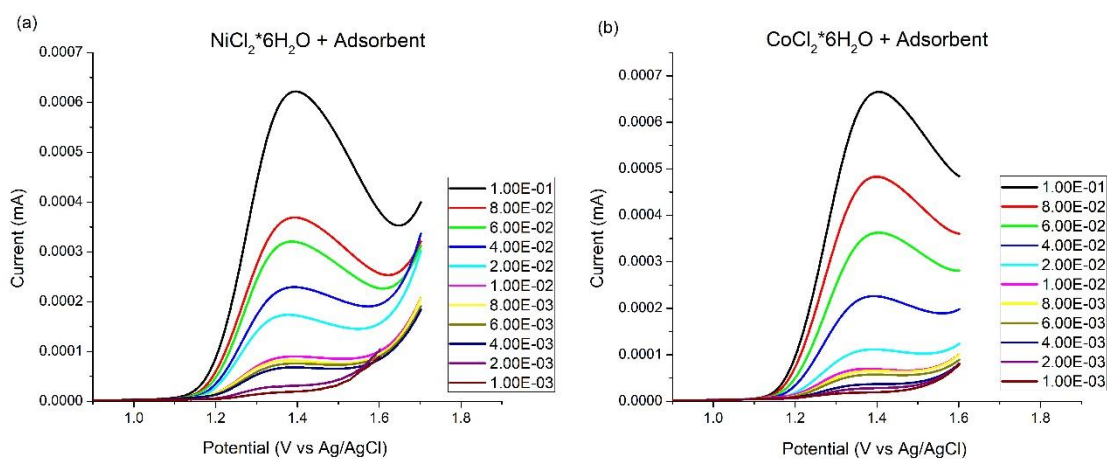


Figure 13. Current curve (a)  $\text{NiCl}_2 \cdot 6\text{H}_2\text{O}$  solution and (b)  $\text{CoCl}_2 \cdot 6\text{H}_2\text{O}$  solution after of adsorption process.

### 5.2.1 Isotherms

As was mentioned, the Isotherm of Adsorption, which is the graphical representation of  $\theta$  vs.  $C$ , can give information about the mechanism of the AP. The fraction  $\theta$  corresponds to the *Adsorbed Amount* /g in mol/g and  $C$  is the final concentration of metal ions in solution. Figure 14 was constructed from the data presented in Table 6 and Table 8 for the UV-Vis and Voltammetry measurements for nickel solutions, respectively, and the Figure 15 from the data in Table 7, and Table 9 for the case of cobalt solutions. The information given in these tables was used in order to obtain the adsorption model that fits best with the experimental data.

From the information given in the Table 6 - Table 9, it is suggested that at low concentrations of metal ion solutions the adsorption percentage is higher than at high concentrations, this because of the adsorbent surface is saturated for the high concentrations, losing its ability for adsorption. In the tables it is observed that at high concentration values there is a trend of almost constant percentages of adsorption, this suggests chemisorption processes where the metal ions are progressively adsorbed. However, at low concentrations it is not observed a monotonic behavior, and taking into account the elevated conductivity exhibited for these samples, for which was required filter it, it is suggested an encapsulation of metal ions by the very small carbonaceous structures dissolved in solution. This fact did not allow the interaction between metal ions with the surface of the solid.

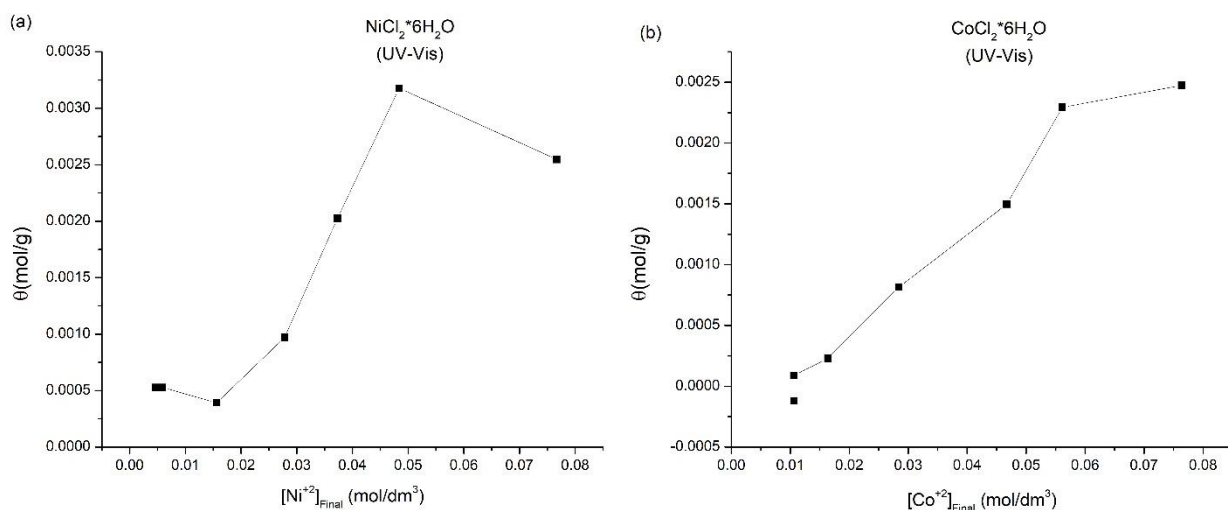


Figure 14. Graphical representation of  $\theta$  vs.  $C$  for (a) Nickel and (b) Cobalt for UV-Vis.

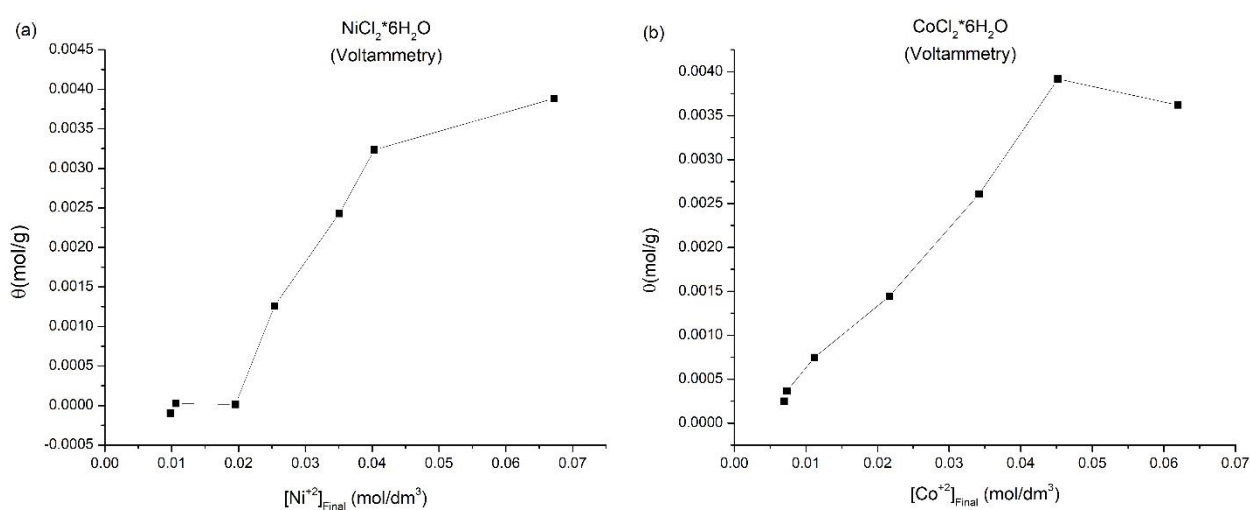


Figure 15. Graphical representation of  $\theta$  vs.  $C$  for (a) Nickel and (b) Cobalt for Voltammetry.

Table 6. Values of  $\text{Ni}^{2+}$  concentration measured by UV-Vis spectroscopy before ( $[\text{Ni}^{2+}]_{\text{Initial}}$ ) and after ( $[\text{Ni}^{2+}]_{\text{Final}}$ ) of the adsorption process from which the adsorbed amount of nickel was determined.

Absorbance (a.u.)	$[\text{Ni}^{2+}]_{\text{Initial}}$ (M)	$[\text{Ni}^{2+}]_{\text{Final}}$ (M)	Adsorbed Amount (mol)	Adsorbent Mass	Adsorbed Amount / $g_{\text{ads}}$ (mol/g)	% Adsorption
0.1507	1.02E-01	0.076694	0.000637	0.25	0.002547	24.93
0.0938	8.02E-02	0.048394	0.000477	0.15	0.003178	39.64
0.0715	5.75E-02	0.037302	0.000304	0.15	0.002024	35.18
0.0524	3.75E-02	0.027803	0.000145	0.15	0.000970	25.86
0.0279	1.95E-02	0.015617	0.000059	0.15	0.000393	20.10
0.0083	1.11E-02	0.005869	0.000105	0.2	0.000527	47.32
0.0059	9.95E-03	0.004675	0.000105	0.2	0.000527	53.00

**Table 7. Values of Ni<sup>2+</sup> concentration measured by voltammetry before ([Ni<sup>2+</sup>]<sub>Initial</sub>) and after ([Ni<sup>2+</sup>]<sub>Final</sub>) of the adsorption process from which the adsorbed amount of nickel was determined.**

Current (mA)	[Ni <sup>2+</sup> ] <sub>Initial</sub> (M)	[Ni <sup>2+</sup> ] <sub>Final</sub> (M)	Adsorbed Amount (mol)	Adsorbent Mass	Adsorbed Amount / g <sub>ads</sub> (mol/g)	% Adsorption
0.000622	1.06E-01	0.067229	0.000971	0.25	0.003884	36.62
0.000369	7.27E-02	0.040311	0.000485	0.15	0.003235	44.52
0.000320	5.94E-02	0.035071	0.000364	0.15	0.002429	40.92
0.000229	3.80E-02	0.025384	0.000189	0.15	0.001259	33.16
0.000174	1.97E-02	0.019543	0.000002	0.15	0.000014	0.70
0.000090	1.09E-02	0.010648	0.000005	0.2	0.000026	2.35
0.000082	8.83E-03	0.009797	-0.000019	0.2	-0.000097	-10.95

As can be seen in the Figure 14-(a) and Figure 15-(a), it seems to exist two different mechanism for the interaction of the Ni<sup>2+</sup> and the adsorbent. For the lowest concentrations values it is suggested a low affinity of the solid with the metal ions, and the slight loss of metal ions from solution can be due to their encapsulation by the suspected hydro-soluble small carbonaceous structure. As the concentration is increased, it is observed a gradual AP until saturation. This behavior is associated with the monolayer formation, which is in agreement with the occurrence of a chemisorption process. This last statement is supported by several experimental observations during the development of the process, such as, change of solution color and the suspicion of hydro-soluble small carbon structures dissolved in solution responsible of the overlapping of the signal at ~400 nm associated with the [Ni(H<sub>2</sub>O)<sub>6</sub>]<sup>2+</sup> complex and the increase of conductivity.

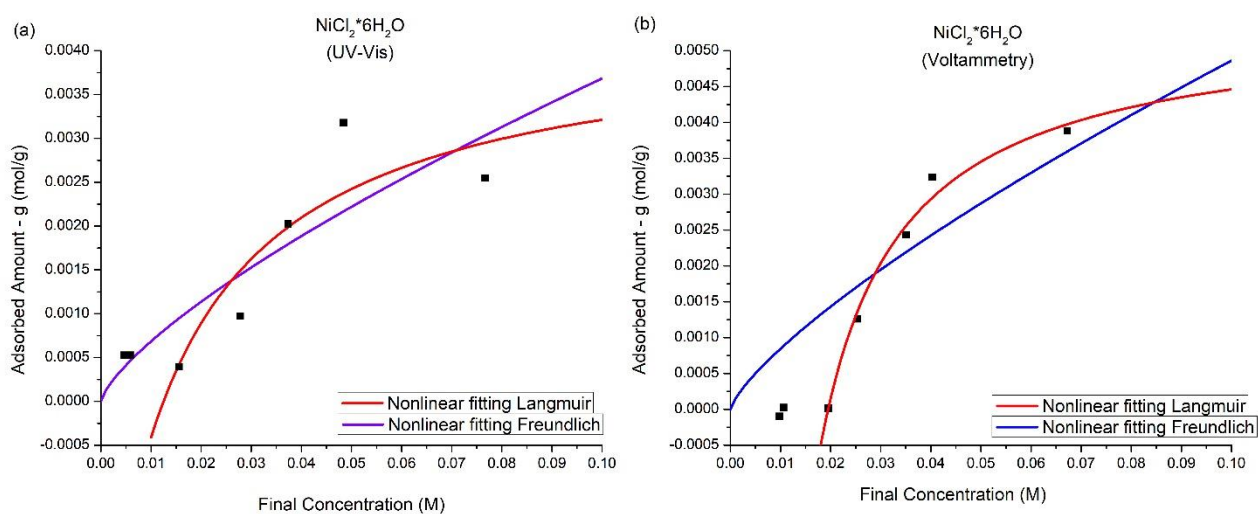


**Figure 16. Nonlinear fitting Langmuir and Freundlich for Ni<sup>2+</sup> solutions from (a) UV-Vis measurements and (b) Voltammetry measurements.**

For the isotherms of adsorption represented in the Figure 14-(a) and Figure 15-(a) were represented the Langmuir and Freundlich models, which are shown in the Figure 16. There is no evidence of a good fit for these models, it is suggested that this behavior is due to presence of a surface chemistry, which the nickel prefers the interaction with the solid, or small carbon structure dissolved, with which it could form complex with tetrahedral geometry, that are more stable than octahedral geometry. When making the different adjustments, the points of lowest value concentration (1E-2 M and 8E-3 M) were eliminated, since they suppose different mechanisms of interaction, the Langmuir model results in a better fit.

### 5.3 Measurements of [Co<sup>2+</sup>] by UV-Spectroscopy and Voltammetry after adsorption process:

Using the equation of CC fits by UV-Vis and Voltammetry methods the concentrations of cobalt ions remaining in solutions were determined, and the Table 8 and Table 9 were constructed. As in the nickel case, the adsorption percentage decreases as the concentration of cobalt solution is increased. The reason can be the same in both cases; the higher concentration implies a solid surface saturation. The last value shown in the Table 8 may be due to the very low value of concentration to be measured, and whose case the sensitivity of the experimental method is compromised.

**Table 8. Values of Co<sup>2+</sup> concentration measured by UV-Vis spectroscopy before ([Co<sup>2+</sup>]<sub>Initial</sub>) and after ([Co<sup>2+</sup>]<sub>Final</sub>) of the adsorption process from which the adsorbed amount was determined.**

<b>Absorbance (a.u.)</b>	<b>[Co<sup>2+</sup>]<sub>Initial</sub> (mol/dm<sup>3</sup>)</b>	<b>[Co<sup>2+</sup>]<sub>Final</sub> (M)</b>	<b>Adsorbed Amount (mol)</b>	<b>Adsorbent Mass</b>	<b>Adsorbed Amount / g<sub>ads</sub> (mol/g)</b>	<b>% Adsorption</b>
0.3791	1.01E-01	0.076374	0.000495	0.2	0.002474	24.47
0.2756	7.91E-02	0.056131	0.000229	0.1	0.002294	29.01
0.2274	6.17E-02	0.046704	0.000150	0.1	0.001496	24.26
0.1337	3.65E-02	0.028379	0.000081	0.1	0.000814	22.28
0.0722	1.86E-02	0.016350	0.000023	0.1	0.000229	12.28
0.0428	1.15E-02	0.010600	0.000013	0.15	0.000090	7.82
0.043	9.43E-03	0.010640	-1.82E-05	0.15	-0.000121	-12.86

**Table 9. Values of  $\text{Co}^{2+}$  concentration measured by Voltammetry before ( $[\text{Co}^{2+}]_{\text{Initial}}$ ) and after ( $[\text{Co}^{2+}]_{\text{Final}}$ ) of the adsorption process from which the adsorbed amount was determined.**

Current (mA)	$[\text{Co}^{2+}]_{\text{Initial}}$ (M)	$[\text{Co}^{2+}]_{\text{Final}}$ (M)	Adsorbed Amount (mol)	Adsorbent Mass	Adsorbed Amount / $g_{\text{ads}}$ (mol/g)	% Adsorption
0.000666	0.098182	0.061981	0.000724	0.2	0.003620	36.87
0.000483	0.084379	0.045199	0.000392	0.1	0.003918	46.43
0.000363	0.060273	0.034193	0.000261	0.1	0.002608	43.27
0.000226	0.036130	0.021678	0.000145	0.1	0.001445	40.00
0.000112	0.018609	0.011156	0.000075	0.1	0.000745	40.05
0.000070	0.010974	0.007337	0.000055	0.2	0.000364	33.14
0.000066	0.009446	0.006959	0.000037	0.2	0.000249	26.32

### 5.3.1 Isotherms

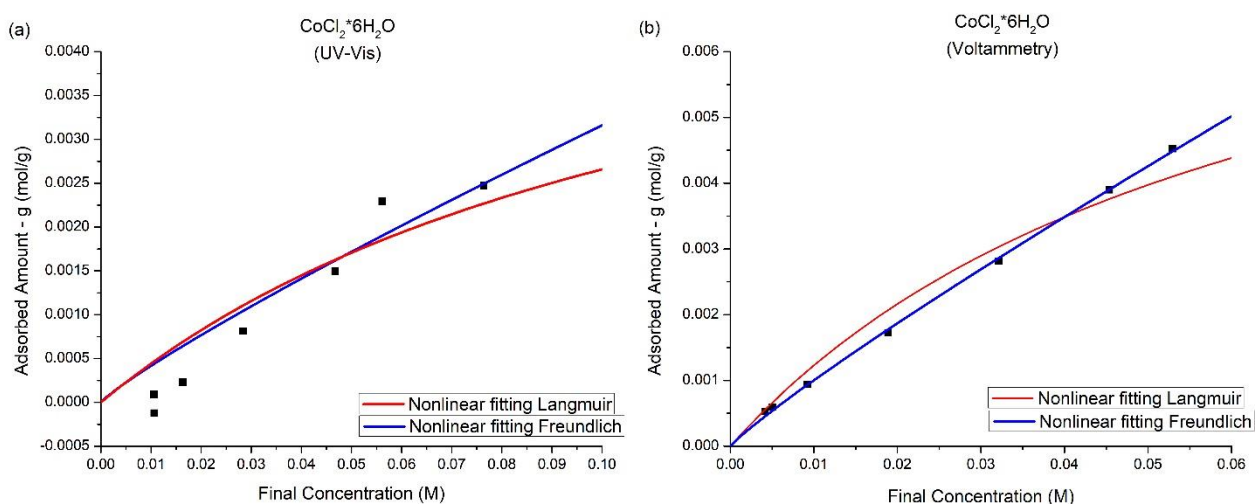


**Figure 17. Nonlinear fitting Langmuir and Freundlich for  $\text{Co}^{2+}$  solutions from (a) UV-Vis measurements and (b) Voltammetry measurements.**

The results of the nonlinear fitting for Langmuir and Freundlich models shown that the data obtained for UV-Vis and Voltammetry are better fitted to the Freundlich model for  $\text{Co}^{2+}$  solutions, which suggests that this is a better representation for this type of bio-adsorbents. On the contrary, the monolayer formation model, on which the Langmuir isotherm is based, is not validated by the experimental data for the adsorption of cobalt ions on these bio-adsorbents. In spite of that for the data obtained by UV-Vis measurements do not proportionate a good fit for any both models, with the current measurements it is obtained a very good fit. This behavior can suggest the multilayer formation, associated with physisorption process. Also it is consistent with the fact that the cobalt prefer to form complex with octahedral geometry, which is the case for  $[\text{Co}(\text{H}_2\text{O})_6]^{2+}$  complex.

### 5.3.2 Other Isotherms - Cobalt Solutions

There are other models that could be a better representation of the heterogeneous system as is the case of the bio-adsorbents. These model result of the combination of Langmuir and Freundlich models. Two of these models correspond to Toth and Sips Isotherm, which were mentioned in the section 4.2. As it can see in the Figure 18, these models are a better representation of the process adsorption for the cobalt ions solutions on the bio-adsorbent evaluated. In the Table 10 it is resumed the values of the fitting regression coefficient, from which is evident that the Sips Isotherm is the better model to represent the AP evaluated for the case of cobalt solutions.

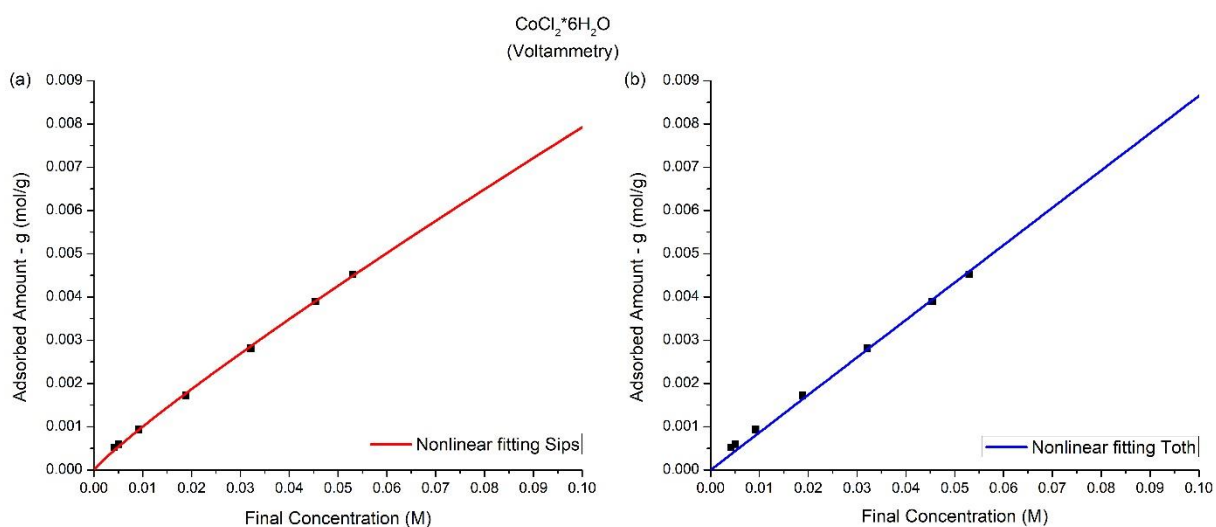


Figure 18. Nonlinear fitting to  $\text{Co}^{2+}$  solutions from voltammetry measurements for (a) Sips model and (b) Toth model.

Table 10. Fitting for the other Isotherms for Cobalt solutions.

Model	Equation	Fitting Coefficient	Fitting Parameters
Sips Isotherm	$\theta = \frac{K_S C^{\frac{1}{n}}}{1 + K_S C^{\frac{1}{n}}}$	0.99972	$K_S = 0.0636272$ $1/n = 0.91219$
Toth Isotherm	$\theta = \frac{C}{(K_T + (C)^n)^{\frac{1}{n}}}$	0.99826	$K_T = 15.098$ $1/n = 0.9$

**Table 11. Percentage removal of heavy metal ions of other methods.**

Processes	% Adsorption	Experimental conditions
Ion exchange	98% Niquel	Sensitive to particles Expensive resins Hydrodynamic conditions <sup>37</sup> .
Membrane filtration	60-90% Niquel	The % of metal removal depends on the membrane used <sup>38</sup> .
Chemical precipitation	97% Niquel	Higher concentrations <sup>39</sup> .
Activated carbon	92.01% to 95.34% Niquel.	At 80°C and contact time of 60 minutes <sup>40</sup> .

Table 11 shows the different percentages of removal of heavy metal ions of other methods, which are higher compared to the percentages obtained in Table 6, Table 7, Table 8, and Table 9. However, the research project simply proposes to evaluate the adsorption capacity of the solid. Although, if the adsorbent was functionalized, a better adsorption rate could be achieved.

## 5.4 Solid Characterization

### X-ray photoelectron spectroscopy (XPS)

Systems such as graphite locate the position of the C1s line with a maximum peak at 284.42 eV and an asymmetry parameter of 0.05 - 0.065, several authors also propose higher excitation energies or bond energies at 120 - 194 eV although these results are still in discussion<sup>28</sup>.

In an analysis of XPS can also be observed oxygen atoms near the surface of the coal, its presence is due to traces of oxygen that are introduced during a process of carbonization or oxygen molecules or water absorbed by the system. The signals of line O1s for porous carbons and carbon nanosheets are observed in 531.9 - 533.3 eV<sup>41</sup>.

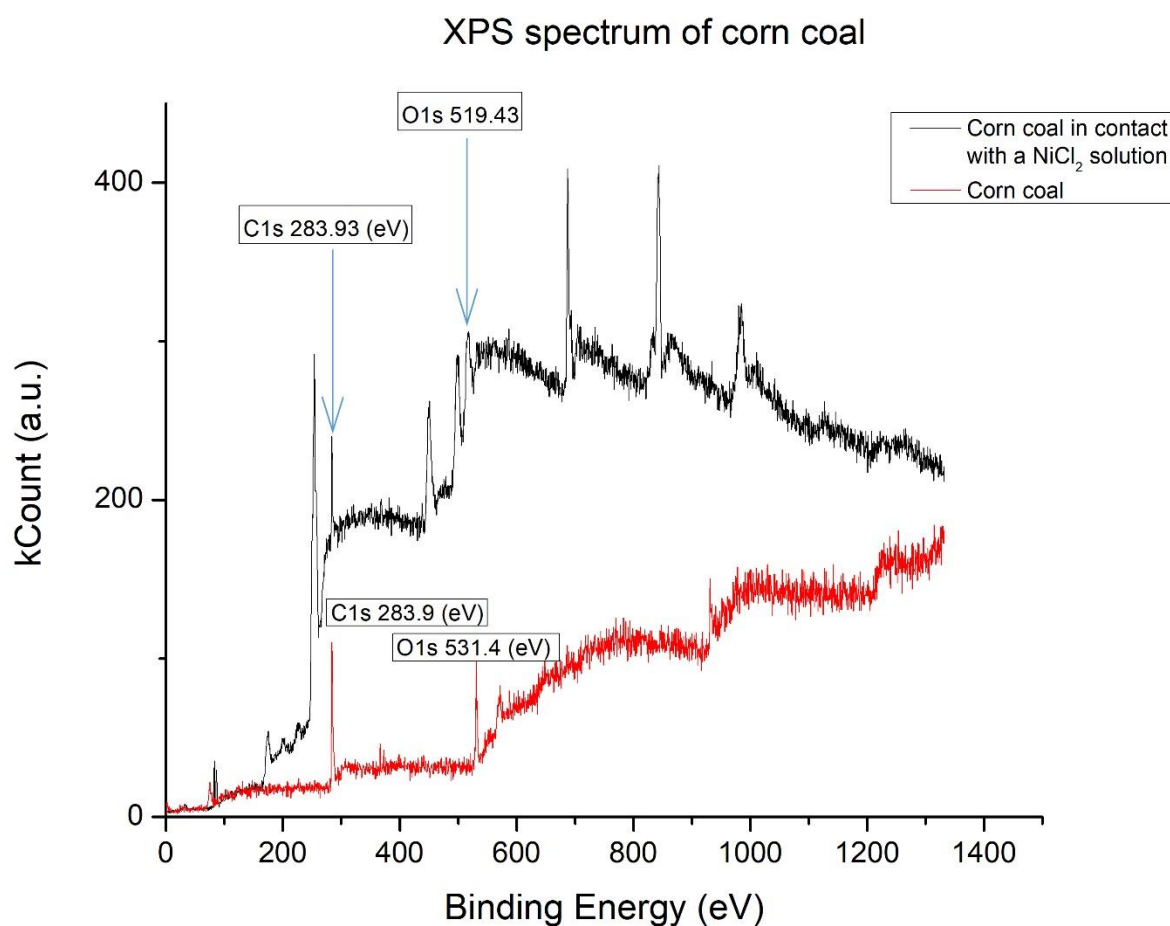


*Figure 19. XPS spectrum of corn coal, C1s and O1s lines.*

The Figure 19 shown the XPS spectrum corn coal sample used as adsorbent (red curve), the spectrum locates the C1s and O1s lines in 283.9 eV and 531.4 eV, respectively, we can see that the values obtained are close to the values that are detailed in the literature but its variation in value can be by

several factors which include signals from the support where the sample was measured and the presence of several layers in the carbon system.

The black curve corresponds to the adsorbent in contact of a  $\text{NiCl}_2$ , several peaks are observed that differ from the red curve. However, in black curve the bands for O1s and for C1s can be observed which are characteristic for carbon structures.

The black curve is divided in different regions in order to identify the different structures that can be presented in the system. These regions correspond to Carbon Region, Oxygen Region, Nickel Region and  $\text{NiCl}_2$  Region, and they are described below.

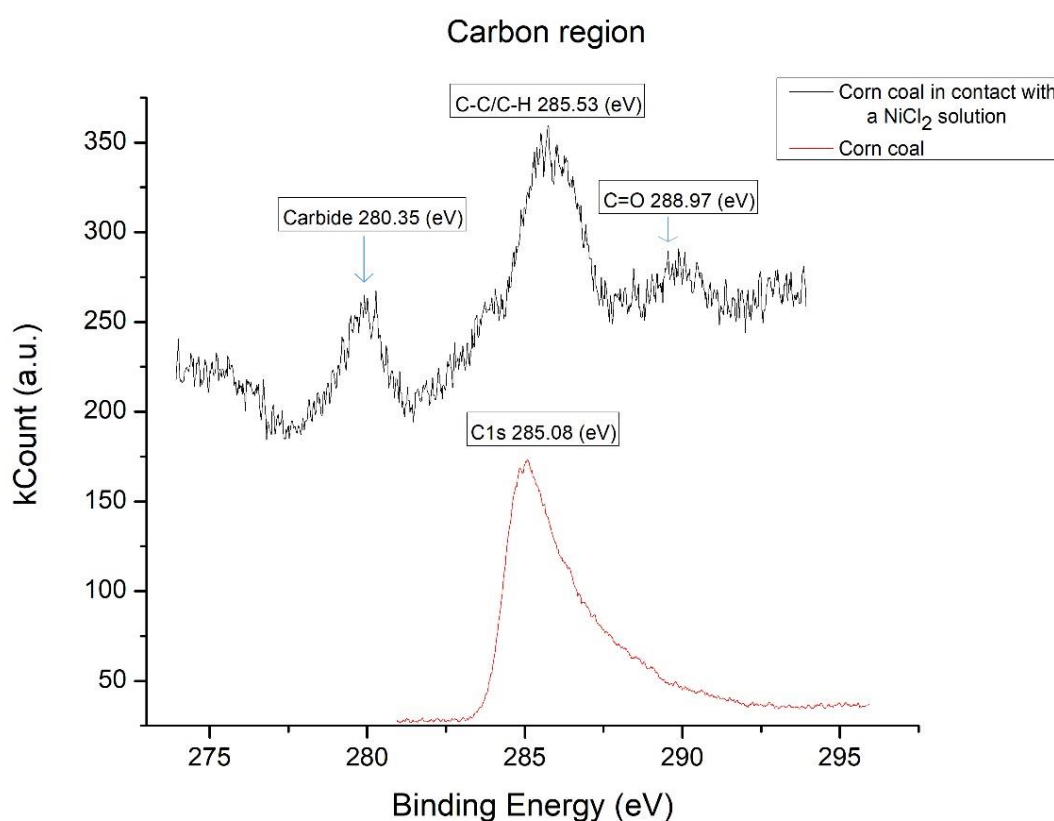


*Figure 20. XPS spectrum of corn coal in the carbon region (C1s).*

In Figure 20 represents the Carbon Region, for which the black curve shown a peak corresponding to C-C or C-H which is located around 285 eV, this value is associated to structured carbonaceous systems, which can be a consequence of the presence of lignin<sup>42</sup>. This peak can also be seen in red curve. This peak still appear for the carbon after adsorption (black curve), but is slightly shifted to ~285.08 eV. Also, in black curve appears a band around 288.97 eV, which can be attributed to the carbonyl region C=O present in the lignin system, affected by the presence of absorbate<sup>42</sup>.

The band occurring at 280.35 eV suggest the presence of nickel carbide due to information obtained given by Goto *et al*, who associates to these species a band at a value of binding energy of 283.6 eV<sup>43</sup>. Although the values are not identical, in the case of the study of Goto et al, the Ni<sub>3</sub>C analyzed to corresponds to a one synthesized by a thermolysis procedure under conditions of high temperature, and the presence of Ni<sub>3</sub>C was evidenced by appearance of a different peak, that appear at lower values than 285.5 eV. Due of this, and to the suggestion given for the Handbook of X-ray Photoelectron Spectroscopy<sup>44</sup>, for the specie Ni<sub>3</sub>C, it is assumed a presumptive formation of carbide species by an autocatalytic reaction from the lignin.

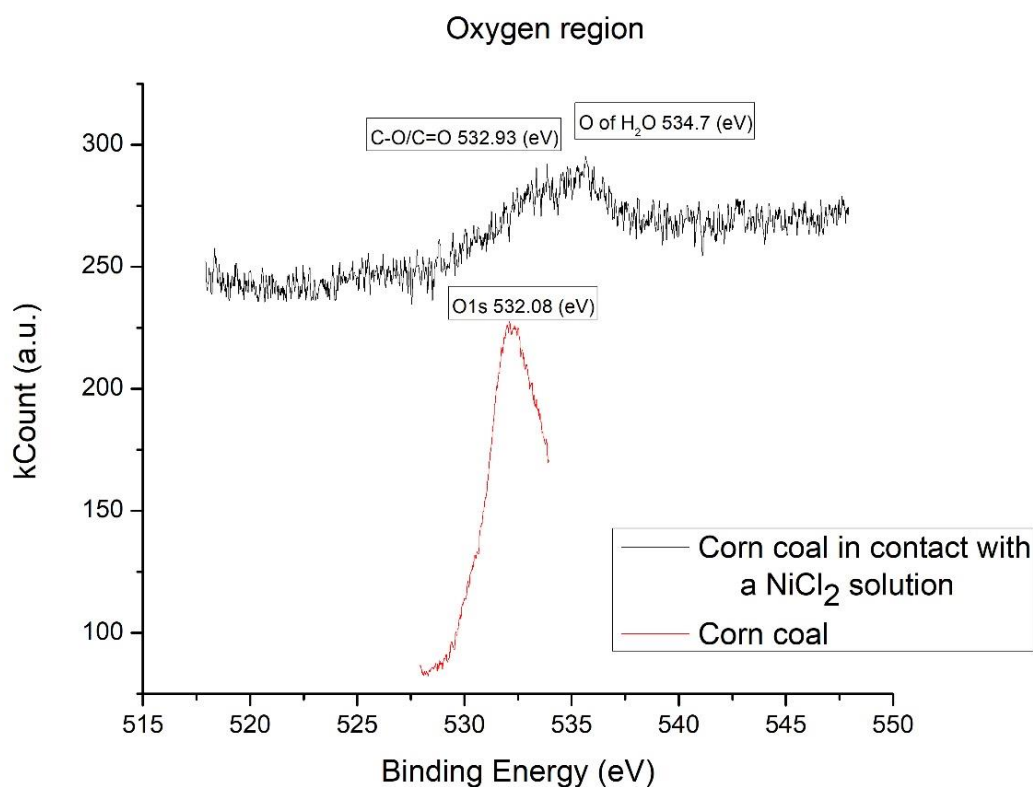


**Figure 21.** XPS spectrum of corn coal in the oxygen region (O1s).

Figure 21 correspond to the Oxygen Region, in which the red curve shown a band around 532.08 eV that it is associated to C-O / C=O bonds. While for the black curve the same band is observed at 532.93 eV. As is indicated in the literature, the shift of this band to values higher than 532 eV has associated a greater contribution of C-O bonds than the C=O bonds<sup>45</sup>. Another signal that is observed in the red line near 534.7 (eV) belongs to the oxygen of water molecules<sup>45</sup>.

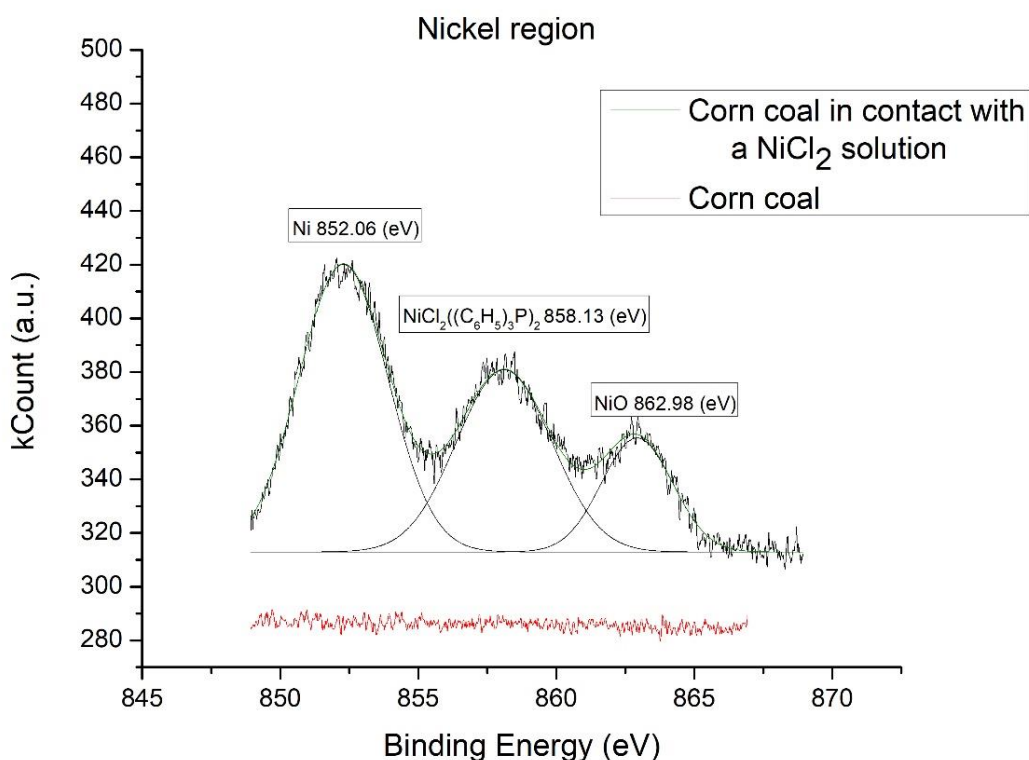


**Figure 22.** XPS spectrum of corn coal in the nickel region (Ni 2p3/2).

Nickel Region is shown in Figure 22, in that the red curve (before the AP) no significant band is observed in the entire interval evaluated. The sample corresponding to after the AP is represented by the black curve, and in that appear several peaks that, according the literature, are associated to several species of nickel. The information found suggest that for metal nickel the XPS band is located at 852.6 eV<sup>43,44,46</sup>, while that the band located around 857 eV is associated with bidentate NiCl<sub>2</sub> species, such as NiCl<sub>2</sub>(Ph<sub>3</sub>P)<sub>2</sub><sup>44</sup>. In addition, NiO presents a set of five peaks, appearing within the interval of Binding Energy of 853.9 eV - 866.5 eV, specifically the highest peaks at 864.2 and 866.5 eV, and the other main signals at 853.9 eV, 855.6 eV and 861.1 eV<sup>47</sup>.

In the spectrum obtained for the sample after the contact with nickel solution (black curve) the most representative bands of the spectrum are indicated in the Figure 22 as those for Ni 852.06 eV, NiCl<sub>2</sub>(Ph<sub>3</sub>P)<sub>2</sub> (or other similar bidentate specie) at 858.13 eV, and NiO 862.98 eV. These bands present a slight shift in relation to the values suggested in the literature. The effects of the electronegativity of neighboring molecules that can affect the binding energy must be taken into consideration<sup>46</sup>.

Several of the obtained bands, such as that associated to NiCl<sub>2</sub>(Ph<sub>3</sub>P)<sub>2</sub> and NiO suggest the depolymerization of lignin in phenolic, aldehyde, and phenolic products. In addition, the presence of

Lewis acid salts such as  $\text{NiCl}_2$  promotes the cleavage of the C-C bonds in aliphatic groups that bind the aromatic units in coal<sup>48</sup>.

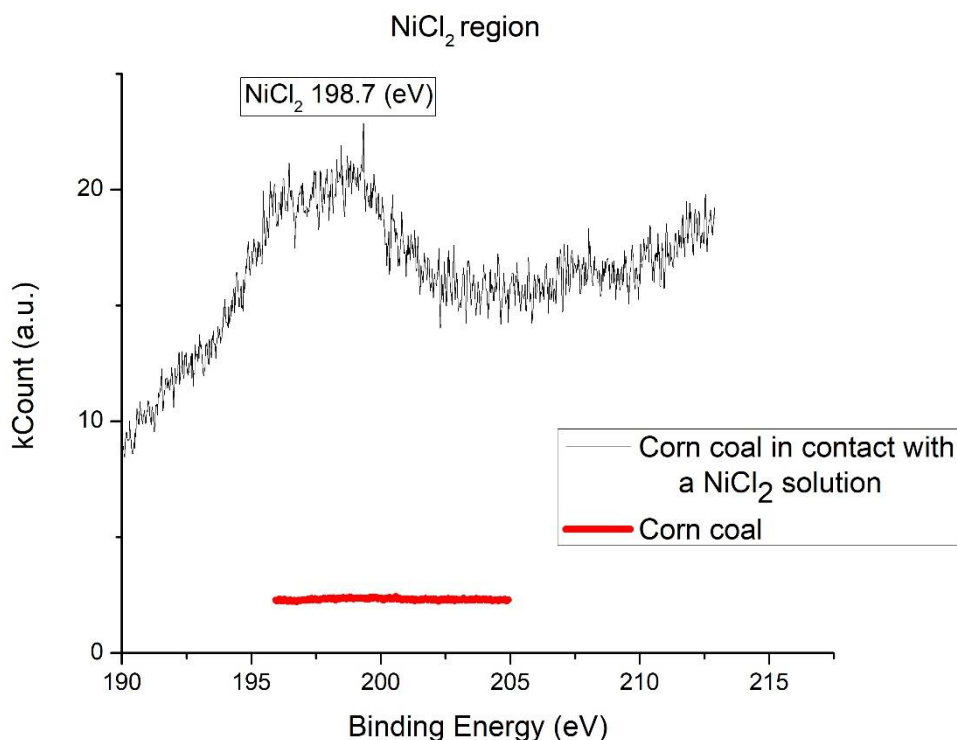


*Figure 23. XPS spectrum of corn coal in the  $\text{NiCl}_2$  region.*

The Figure 23 shown the  $\text{NiCl}_2$  Region for both samples of bio-adsorbent, the original one and that in contact with nickel ion solution. The almost flat red curve evidences the absence of this specie before the AP. On the contrary, the presence of a peak near at 198.7 eV (BE) corresponds to the  $\text{NiCl}_2$  species<sup>44</sup>. This suggests that part of all the nickel present is being deposited on the surface in the form of  $\text{NiCl}_2$ , perhaps forming an octahedral complex with the water present in the sample, without the formation of chemical bonds.

The spectra obtained for the bio-adsorbent in contact with nickel solutions point to possibility of chemisorption process occurred for the nickel case, which is in concordance with the previously information indicated related with the analysis of isotherms of adsorption.

Unfortunately, the samples corresponding to the cobalt case could not be analyzed by the XPS experiments. This information would be key to strengthen the mechanism suggested.

## Raman spectroscopy

In this analysis, the peaks that are well known for characterizing graphitic materials are G (graphite peaks) and D (disordered) bands. For a sample of pure graphite, the appearance of the G band is due to the relative motion of  $sp^2$  hybridized C atom and the peak D is related to the breathing vibrational mode of the six-membered rings. These bands in a Raman spectrum correspond to the peaks with greater intensity, the G band appears around  $1585\text{cm}^{-1}$  and near  $1350\text{ cm}^{-1}$  appears the D band<sup>49,50</sup>.

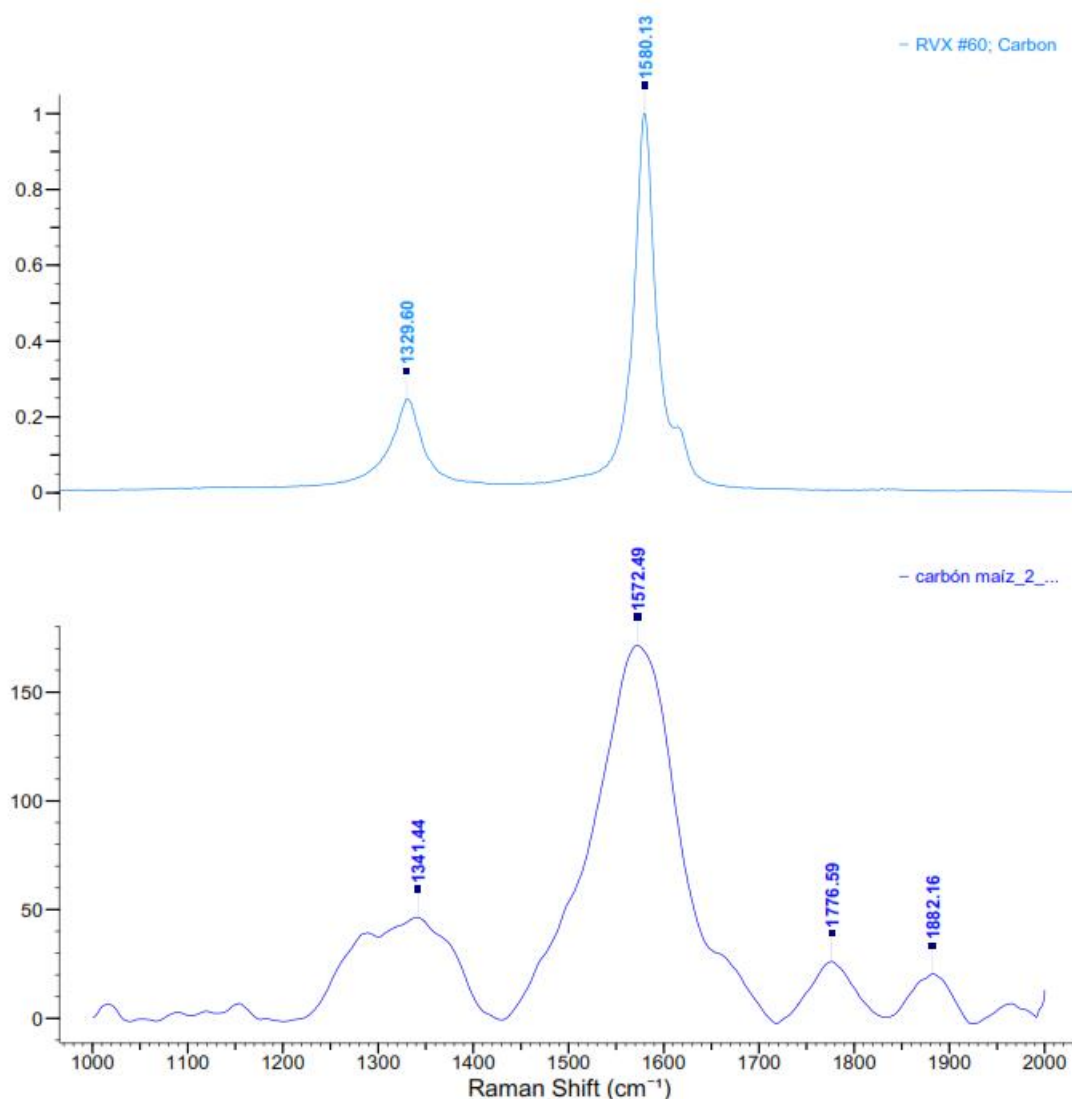


*Figure 24. Comparison of Carbon Raman spectra of the database (top image) versus corn coal (bottom image) used as adsorbent.*

In Figure 24, the G and D bands of the graphitic materials for the bio-adsorbent prepared from corn coal appear with a slight shift compared to the value of the carbon in the database. This is possibly due to the fact carbonization process, to which the corn stem was subjected, resulted in amorphous carbon. Other peaks observed in the spectrum can be attributed to some compounds found in the adsorbent, such as lignin and cellulose, according the information given in the Table 12 for the case of lignin.

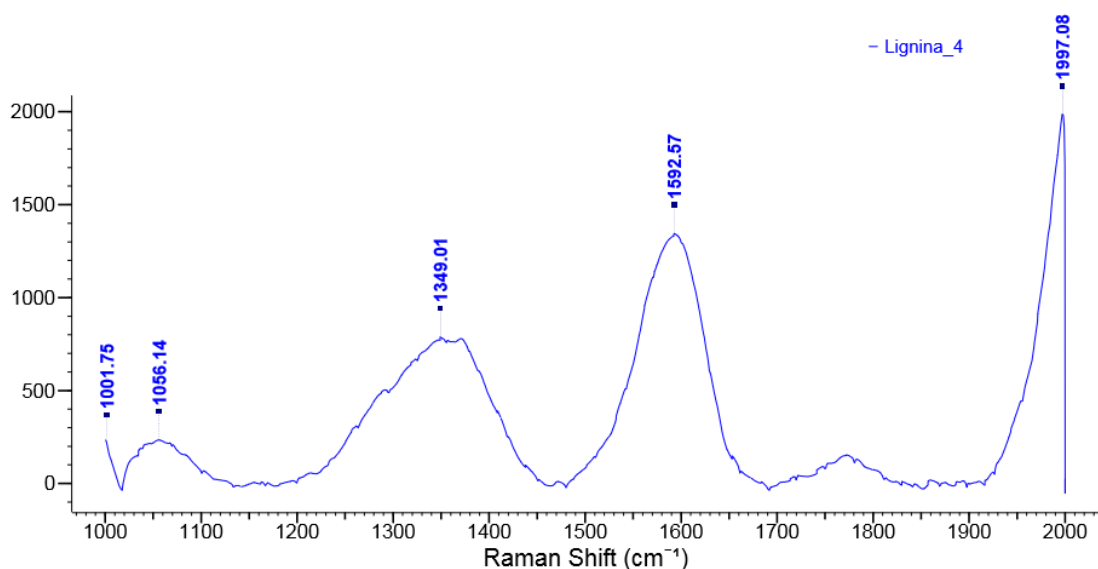


**Figure 25. Raman spectrum for lignin extracted in the laboratory.**

Several aspects must be taken into consideration in relation to the Raman spectrum of lignin which include several lignin structures, substructures, and functional groups<sup>51</sup>. In view of this correspondence, it was extracted the lignin following the procedure reported by Watkins *et al*<sup>52</sup>, and it was also analyzed by Raman spectroscopy, whose spectrum it is shown in the Figure 25. According to the bands appearing in the spectrum, it gives the impression that the bio-adsorbent prepared is mainly composed of lignin, although the absence of a couple of peaks appearing in the spectrum of the bio-adsorbent shown in the Figure 24 (bottom image), could be indicate that some cellulosic compounds are also present. Also, the shift exhibited for the main bands in the bio-adsorbent compared with those for lignin could be consistent with the presence of the cellulose. Moreover, the slight shift of the peaks in the spectrum of lignin with respect to those values indicated in the Table 12, it give the idea that the extraction and purification process of the lignin obtained in the laboratory should be taken into account.

The structure of lignin has several compounds in its structure but according to the obtained Raman spectrum, several bands can be observed based on the tabulated values for the lignin Raman spectra Table 12<sup>51</sup>.

**Table 12. Raman spectra lignin band positions (cm<sup>-1</sup>). Taken from Umesh<sup>51</sup>.**

Band positions (cm <sup>-1</sup> )	Assignments
975 – 984 (vw-sh)	CCH and –HC=CH- deformation
1031 – 1037 (w-m)	C-O of aryl-O-CH <sub>3</sub> and aryl-OH
1088 – 1089 (w)	Out of phase C-C-O stretch of phenol
1331 – 1334 (m-s)	Aliphatic O-H bending
1363 – 1373 (sh)	C-H bend in R <sub>3</sub> C-H
1501 – 1508 (vw)	Aromatic ring stretch, asymmetric
1595 – 1597 (vs)	Aromatic ring stretch, symmetric
1620 – 1621 (sh)	C=C stretch of coniferaldehyde/sinapaldehyde
1661 – 1664 (s)	C=C coniferyl alcohol + C=O coniferaldehyde

Note: vs is very strong; s is strong; m is medium; w is weak; vw is very weak; and sh is shoulder. Band intensities are relative to other peaks in the spectrum.

A study of the incorporation of nickel on the carbonaceous surface of the bio-adsorbent through Raman Spectroscopy results in the spectrum shown in the Figure 26 for the NiCl<sub>2</sub>\*6H<sub>2</sub>O 8E-2 M sample. As is suggested by the analysis of XPS spectra, there is a possible formation of species such as nickel carbide; it could be reinforced with the Raman spectrum of the sample.

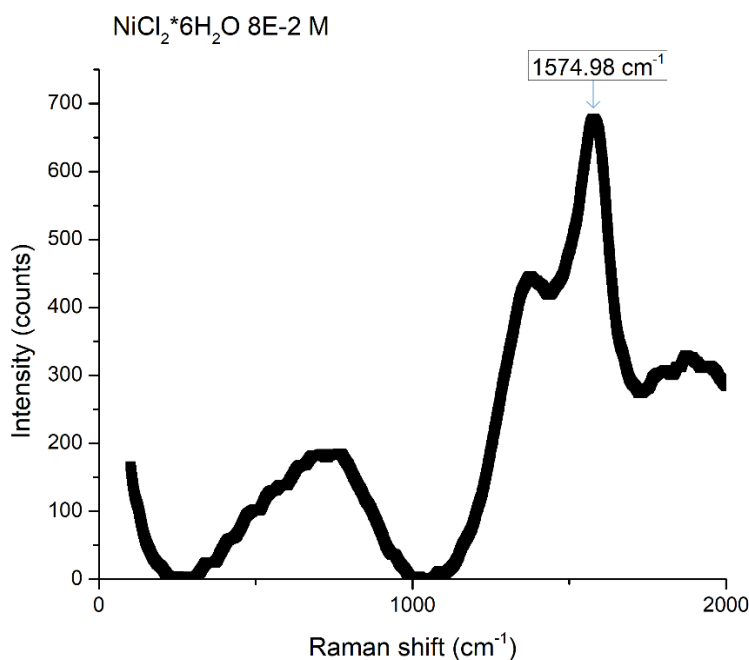


**Figure 26. Raman spectrum of NiCl<sub>2</sub>\*6H<sub>2</sub>O 8E-2 M sample after the adsorption process.**

When doping an a-C:H film with a relative concentration of nickel, a significant change occurs in the G and D bands. An enlargement of the bands is observed for the higher concentration of the metal in the film, the greater the degree of enlargement of the G and D bands and the ratio of the intensity  $I(D) / I(G)$  decreases. The position of the G peak is affected and it is positioned below the peak of crystalline graphite (Figure 27)<sup>53</sup>.

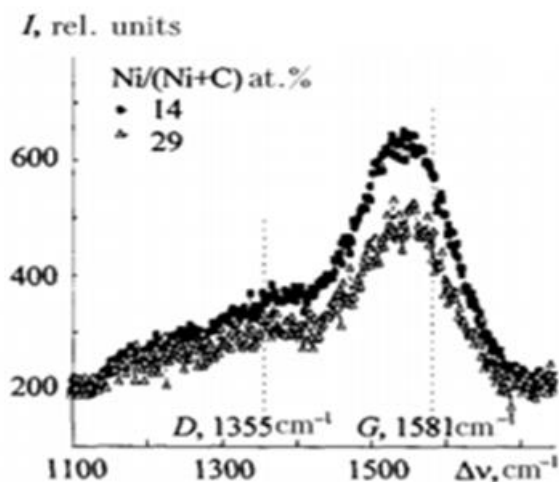


Figure 27. Raman spectrum of hydrogen-containing a-C:H/Ni film. Taken from Uglov<sup>53</sup>.

When observing Figure 26, the positioning of the G band is observed at  $1574.98 \text{ cm}^{-1}$ ; a lower value than the peak location of G band of pure graphite ( $1581\text{-}1585 \text{ cm}^{-1}$ ). In addition, a notable enlargement of the bands is observed, which could be suggest by the presence of nickel carbide species.

## 6. CONCLUSIONS AND RECOMMENDATIONS:

- It is shown that environmental toxic metal contaminants, such as  $\text{Ni}^{2+}$  and  $\text{Co}^{2+}$ , can be successfully removed. Up to ~30 % removal can be achieved for nickel and up to ~ 40% for cobalt. Although in the literature the percentages of removal of metals, using more sophisticated materials are higher than that obtained with the adsorbent developed in this research work, it was possible to evaluate the removal capacity of metals from the adsorbent. Also, if the adsorbent is functionalized a better adsorption percentage could be achieved.
- The UV-Vis and Voltammetry methods were used to choose one among them with the lowest and better sensitivity. However, both methods have the same sensitivity limitation. Moreover, a similar adsorption capacity was obtained from them. However, both methods supported the proposed mechanisms.
- For the nickel case, the experimental data with which was represented the isotherm of adsorption suggest the presence of two mechanisms for the interaction between the nickel species and the carbonaceous surface of the bio-adsorbent. The first one is associated with the possible encapsulation of the nickel by very small hydro-soluble carbonaceous structures dissolved in solution. Another mechanism it seems to be associated with a chemisorption process, which is supported by the fit of the experimental data with that model that supposes a monolayer formation, that is, the Langmuir model.
- The presence of different species of nickel evidenced by XPS and Raman spectroscopy analysis supports the proposed physisorption and chemisorption processes. Some of these species correspond to species that only could be formed by chemical reaction, implying formation of coordinate covalent bond, and even the reduction of the nickel ion.
- The characterization of the solid indicates the presence of lignin in the bio-adsorbent system. The carbonaceous structure of the solid leads to an interesting surface chemistry that suggest the reduction of Ni and possibly formation nickel carbide structures, perhaps by an autocatalytic reaction between the nickel ion and the carbonaceous structure of solid.
- For the case of cobalt, the model of the Freundlich Isotherm and Sips Isotherm are those that better fits with the experimental data. These models suggest that the AP can be described by a mechanism involving the formation of multilayer, also that the adsorbent evaluates is considered an energetically heterogeneous system.

## 7. BIBLIOGRAPHY:

- (1) Norma de calidad ambiental y de descarga de efluentes : recurso agua. Criterios de Calidad Admisibles Para La Preservación de La Flora Y Fauna En Aguas Dulces, Fría O Cálidas En Aguas Marinas Y Estuarinas. **2010**, 286–339.
- (2) Núñez, L. T. Texto Unificado de Legislación Ambiental Secundaria (TULSMA). **2013**, No. 97, 6–26.
- (3) Correa, M.; Bolaños, M.; Rebolledo, E.; Rubio, D.; Salinas, R. *Análisis Del Contenido de Metales En Aguas, Sedimentos Y Peces En La Cuenca Del Río Santiago, Provincia de Esmeraldas, Ecuador.*; 2015; pp 1–11.  
[https://doi.org/http://repositorio.educacionsuperior.gob.ec/bitstream/28000/4911/2/anexo 2 - an% c3% 81lisis del contenido de metales en aguas% 2c sedimentos y peces - prov. esmeraldas.pdf](https://doi.org/http://repositorio.educacionsuperior.gob.ec/bitstream/28000/4911/2/anexo%202-an%C3%81lisis%20del%20contenido%20de%20metales%20en%20aguas%20c%20sedimentos%20y%20peces%20-%20prov.%20esmeraldas.pdf).
- (4) Albornoz, P.; Andrade, M.; Araujo, P.; Gómez, D.; Mejía, D.; Pohlenz, A.; Torres, F.; Morales, M. *Informe Sobre El Estado Del Medio Ambiente*; 2008; pp 1–105.
- (5) Bhardwaj, V.; Kumar, P.; Singhal, G. Toxicity of Heavy Metals Pollutants in Textile Mills Effluents. *Int. J. Sci. Eng. Res.* **2014**, 5 (7), 664–666.
- (6) Morais, S.; Garcia, F. Heavy Metals and Human Health. In *Environmental Health - Emerging Issues and Practice*; Oosthuizen, J., Ed.; InTech, 2010; pp 229–246.
- (7) Raouf, A. Removal of Heavy Metals from Industrial Waste Water by Biomass-Based Materials : A Review. *J. Pollut. Eff. Control* **2017**, 5 (1), 1–13. <https://doi.org/10.4172/2375-4397.1000180>.
- (8) Gupta, V. K. Bioadsorbents for Remediation of Heavy Metals : Current Status and Their Future Prospects. *Environ. Eng. Res.* **2015**, 20 (1), 1–18.
- (9) Králik, M. Adsorption, Chemisorption, and Catalysis. *Chem. Pap.* **2014**, 68 (12), 1–14. <https://doi.org/10.2478/s11696-014-0624-9>.
- (10) Tripathi, A.; Ranjan, M. R. Heavy Metal Removal from Wastewater Using Low Cost Adsorbents Bior Emediation & Biodegradation. *J. Bioremediation Biodegrad.* **2015**, 6 (6). <https://doi.org/10.4172/2155-6199.1000315>.
- (11) Bamdad, H.; Hawboldt, K.; Macquarrie, S. A Review on Common Adsorbents for Acid Gases Removal : Focus on Biochar. *Renew. Sustain. Energy Rev.* **2017**, No. October 2016, 1–16. <https://doi.org/10.1016/j.rser.2017.05.261>.

- (12) Ghosh, P. *Colloid and Interface Science*; PHI Learning Private Limited: New Delhi, 2009.
- (13) Ayawei, N.; Ebelegi, A. N.; Wankasi, D. Modelling and Interpretation of Adsorption Isotherms. *J. Chem.* **2017**, 2017.
- (14) Bruggen, B. Van Der. Freundlich Isotherm. *Encycl. Membr.* **2003**, 1–2.  
<https://doi.org/10.1007/978-3-642-40872-4>.
- (15) Demirbas, A. Heavy Metal Adsorption onto Agro-Based Waste Materials : A Review. *J. Hazard. Mater.* **2008**, 157 (2–3), 220–229. <https://doi.org/10.1016/j.jhazmat.2008.01.024>.
- (16) Volesky, B. Detoxification of Metal-Bearing Effluents : Biosorption for the next Century. *Hydrometallurgy* **2001**, 2–3 (59), 203–216.
- (17) Guo, X.; Zhang, S.; Shan, X. Adsorption of Metal Ions on Lignin. *J. Hazard. Mater.* **2008**, 151, 134–142. <https://doi.org/10.1016/j.jhazmat.2007.05.065>.
- (18) Lalvani, S. B., Wiltowsky, T. S., Murphy, D., Lalvani, L. S. Metal Removal from Process Water by Lignin. *Environ. Technol.* **1997**, 18 (11), 1163–1168.  
<https://doi.org/10.1080/09593331808616636>.
- (19) Chávez, M. LIGNINA , ESTRUCTURA Y APLICACIONES : MÉTODOS DE DESPOLIMERIZACIÓN PARA LA OBTENCIÓN DE DERIVADOS AROMÁTICOS DE INTERÉS INDUSTRIAL LIGNIN , STRUCTURE AND APPLICATIONS : DEPOLYMERIZATION METHODS FOR. *Av. en Ciencias e Ing.* **2013**, 4 (4), 15–46.
- (20) Naseer, A.; Jamshaid, A.; Hamid, A.; Ghauri, M.; Iqbal, J.; Rafiq, S. Lignin and Lignin Based Materials for the Removal of Heavy Metals from Waste Water-An Overview. *An Overview. Zeitschrift Für Phys. Chemie* **2018**.
- (21) Demirbas, A. Adsorption of Lead and Cadmium Ions in Aqueous Solutions onto Modified Lignin from Alkali Glycerol Delignification. *J. Hazard. Mater.* **2004**, 109, 221–226.  
<https://doi.org/10.1016/j.jhazmat.2004.04.002>.
- (22) Brebu, M.; Vasile, C. THERMAL DEGRADATION OF LIGNIN – A REVIEW. *Cellul. Chem. Technol.* **2010**, 44 (9), 353–363.  
[https://doi.org/http://www.cellulosechemtechnol.ro/pdf/CCT9\(2010\)/P.353-363.pdf](https://doi.org/http://www.cellulosechemtechnol.ro/pdf/CCT9(2010)/P.353-363.pdf).
- (23) Society, R.-A. the C. Ultraviolet - Visible Spectroscopy (UV). *R. Soc. Chem.* **2009**.
- (24) Speiser, B. Linear Sweep and Cyclic Voltammetry. *Encyclopedia of Electrochemistry*; 2007; pp 81–104.
- (25) Parker, V. D. Linear Sweep and Cyclic Voltammetry. *Compr. Chem. Kinet.* **1986**, 26, 145–

202.

- (26) Bard, A. J.; Faulkner, L. R.; Swain, E.; Robey, C. *Fundamentals and Applications*, Second ed.; John Wiley & Sons, INC: Texas, 2001.
- (27) Franinović, M. X-Ray Photoelectron Spectroscopy. *Seminar* **2012**.
- (28) Susi, T.; Pichler, T.; Ayala, P. X-Ray Photoelectron Spectroscopy of Graphitic Carbon Nanomaterials Doped with Heteroatoms. *J. Nanotechnol.* **2015**, *6*, 177–192.  
<https://doi.org/10.3762/bjnano.6.17>.
- (29) Barlow, A. J.; Popescu, S.; Artyushkova, K.; Scott, O.; Sano, N.; Hedley, J.; Cumpson, P. J. Chemically Specific Identification of Carbon in XPS Imaging Using Multivariate Auger Feature Imaging (MAFI). *Carbon N. Y.* **2016**, *107*, 190–197.  
<https://doi.org/10.1016/j.carbon.2016.05.073>.
- (30) Wang, Q. Raman Spectroscopic Characterization and Analysis of Agricultural and Biological Systems by. *Grad. Theses Diss.* **2013**, 1–158.
- (31) Kauffmann, T. Use of Stokes and Anti - Stokes Raman Scattering for New Applications. *J. Raman Spectrosc.* **2018**, No. October, 1–7. <https://doi.org/10.1002/jrs.5523>.
- (32) Huheey, J.; Keiter, E.; Keiter, R. *Inorganic Chemistry - Principles of Structure and Reactivity 4th Ed.*, 4th ed.; HarperCollins College Publishers: New York, 1993.
- (33) Liu, W.; Migdisov, A.; Williams-jones, A. The Stability of Aqueous Nickel ( II ) Chloride Complexes in Hydrothermal Solutions : Results of UV – Visible Spectroscopic Experiments. *Geochim. Cosmochim. Acta* **2012**, *94*, 276–290. <https://doi.org/10.1016/j.gca.2012.04.055>.
- (34) Petkova, P.; Nedkov, V.; Preslavsky, K.; Str, U. Behavior of  $\text{Co}^{2+}$  Cations in the Aqueous and Alcoholic Solution of  $\text{CoCl}_2 \cdot 6\text{H}_2\text{O}$ . *Acta Phys. Pol. A* **2013**, *123* (2), 207–208.  
<https://doi.org/10.12693/APhysPolA.123.207>.
- (35) Madam, R. *Chemistry for Degree Students*, 3rd ed.; S. Chand & Company: New Delhi, **2014**.
- (36) Dong, Y.; Ma, Y.; Lui, Y.; Feng, X.; Zhan, J. Construction of 3D Architectures with  $\text{Ni}(\text{HCO}_3)_2$  Nanocubes Wrapped by Reduced Graphene Oxide for LIBs: Ultrahigh Capacity, Ultrafast Rate Capability and Ultralong Cycle Stability. *R. Soc. Chem.* **2018**.
- (37) Zewail, T. M. Kinetic Study of Heavy Metal Ions Removal by Ion Exchange in Batch Conical Air Spouted Bed. *ALEXANDRIA Eng. J.* **2015**, *54* (1), 83–90.  
<https://doi.org/10.1016/j.aej.2014.11.008>.
- (38) Nagy, E. Removal of Zinc and Nickel Ions by Complexation Membrane Filtration Process

from Industrial Wastewater. **2009**, 240 (1–3), 2–6.

<https://doi.org/10.1016/j.desal.2007.11.073>.

- (39) Mahmood, M.; Barbooti, M.; Balasim, A.; Altameemi, A.; Najah, M.; Al-Shuwaiki, N. Removal of Heavy Metals Using Chemicals Precipitation. *Eng. Technol. J.* **2011**, 29.
- (40) Abdulrazak, S.; Sani, K. H. H. M. Evaluation of Removal Efficiency of Heavy Metals by Low-Cost Activated Carbon Prepared from African Palm Fruit. *Appl. Water Sci.* **2016**, 7 (6), 3151–3155. <https://doi.org/10.1007/s13201-016-0460-x>.
- (41) Yuan, K. Carbon-Based Materials for Energy Conversion and Storage. *Bergische Univ. Wuppertal* **2017**.
- (42) Stark, N. M.; Yelle, D. J.; Agarwal, U. P. *4 Techniques for Characterizing Lignin*; Elsevier Inc., 2016. <https://doi.org/10.1016/B978-0-323-35565-0.00004-7>.
- (43) Goto, Y.; Taniguchi, K.; Omata, T.; Otsuka-yao-matsuo, S. Formation of Ni<sub>3</sub>C Nanocrystals by Thermolysis of Nickel Acetylacetonate in Oleylamine : Characterization Using Hard X-Ray Photoelectron Spectroscopy. *Chem. Mater.* **2008**, No. 2, 4156–4160.
- (44) Moulder, John., Stickle, William., Sobol, Peter., Bomben, K. *Handbook of X-Ray Photoelectron Spectroscopy*; Chastain, J., Ed.; Perkin-Elmer Corporation., Physical Electronics Division: Minnesota, 1992.
- (45) Rojas, J. V; Toro-gonzalez, M.; Molina-higgins, M. C.; Castano, C. E. Facile Radiolytic Synthesis of Ruthenium Nanoparticles on Graphene Oxide and Carbon Nanotubes. *Mater. Sci. Eng. B* **2016**, 205, 28–35. <https://doi.org/10.1016/j.mseb.2015.12.005>.
- (46) Grosvenor, A. P.; Biesinger, M. C.; Smart, R. S. C.; McIntyre, N. S. New Interpretations of XPS Spectra of Nickel Metal and Oxides. *Surf. Sci.* **2006**, 600 (9), 1771–1779. <https://doi.org/10.1016/j.susc.2006.01.041>.
- (47) Marchetti, L.; Miserque, F.; Pijolat, M. XPS Study of Ni-Base Alloys Oxide Films Formed in Primary Conditions of Pressurized Water Reactor. *Surf. Interface Anal.* **2015**, 47 (5), 632–642. <https://doi.org/10.1002/sia.5757>.
- (48) Guvenatam, B. *Catalytic Pathways for Lignin Depolymerization*; Eindhoven: Technische Universiteit Eindhoven, 2019.
- (49) Jorio, A. Raman Spectroscopy in Graphene-Based Systems : Prototypes for Nanoscience and Nanometrology. *Int. Sch. Res. Netw.* **2012**, 2012 (2). <https://doi.org/10.5402/2012/234216>.
- (50) Furlan, A.; Lu, J.; Hultman, L.; Jansson, U.; Magnuson, M. Crystallization Characteristics and Chemical Bonding Properties of Nickel Carbide Thin Film Nanocomposites. *J. Phys.*

2014, 415501.

- (51) Umesh, P.; James, D.; Sally, A. FT – Raman Investigation of Milled-Wood Lignins : Softwood , Hardwood , and Chemically Modified Black Spruce Lignins. *J. Wood Chem. Technol.* **2011**, *31*, 324–344. <https://doi.org/10.1080/02773813.2011.562338>.
- (52) Watkins, D.; Hosur, M.; Tcherbi-narteh, A.; Jeelani, S. Extraction and Characterization of Lignin from Different Biomass Resources &. *Integr. Med. Res.* **2014**, No. x x, 1–7. <https://doi.org/10.1016/j.jmrt.2014.10.009>.
- (53) Uglov, V. V; Kuleshov, A. K.; Samtsov, M. P.; Astashinsakaya, M. V. RAMAN LIGHT SCATTERING IN HYDROGENATED METAL-CARBON COMPOSITE FILMS. *J. Appl. Spectrosc.* **2006**, *73* (3), 344–348.

## 8. ANNEX:

**RECEIPT DATE:** Urcuquí, June 14, 2019.

Dolores Lastenia Parra Quisahuano

## NAME AND SIGNATURE

Hortensia María Rodríguez Cabrera

**DEAN'S SCHOOL**